

Radboud Universiteit



Subtle quantum physics probed by STM: Examples and Lessons

Mikhail Katsnelson



Institute for Molecules and Materials

Outline

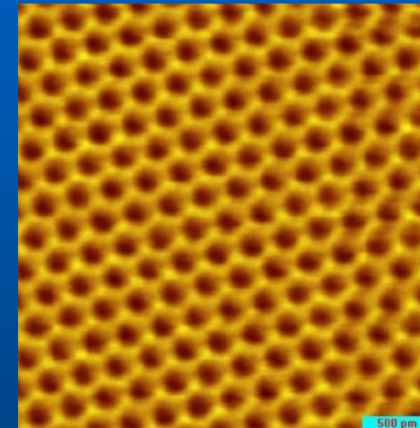
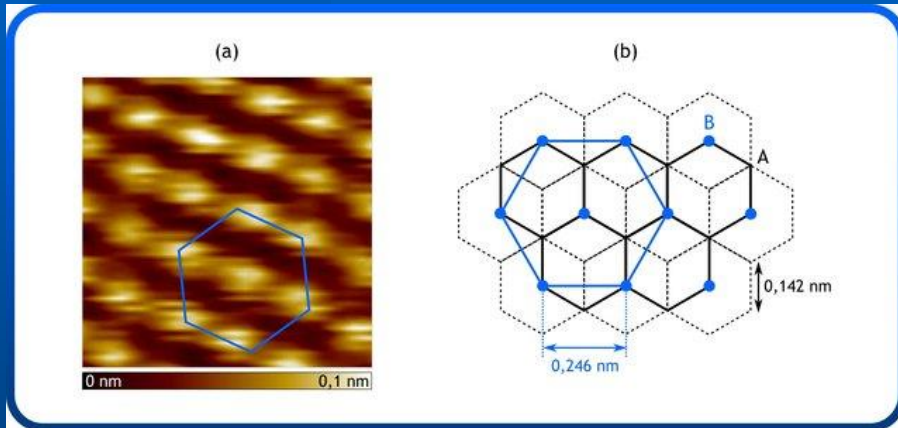
- 1. Many-body quantum physics: Orbital Kondo resonance on Cr(001) surface**
- 2. Topology and geometry matters: Berry phase manifestation in Friedel oscillations at graphene surface**
- 3. Complexity of magnetic patterns and self-induced spin-glass state: Spin-polarized STM in Nd**

Focus on interplay of theory and experiments

Epigraph

Whether you can observe a thing or not depends on the theory which you use. It is theory which decides what can be observed.

(A. Einstein)



STM image and crystal structure of graphite (thesis L. Scifo)

<https://tel.archives-ouvertes.fr/tel-00196927>

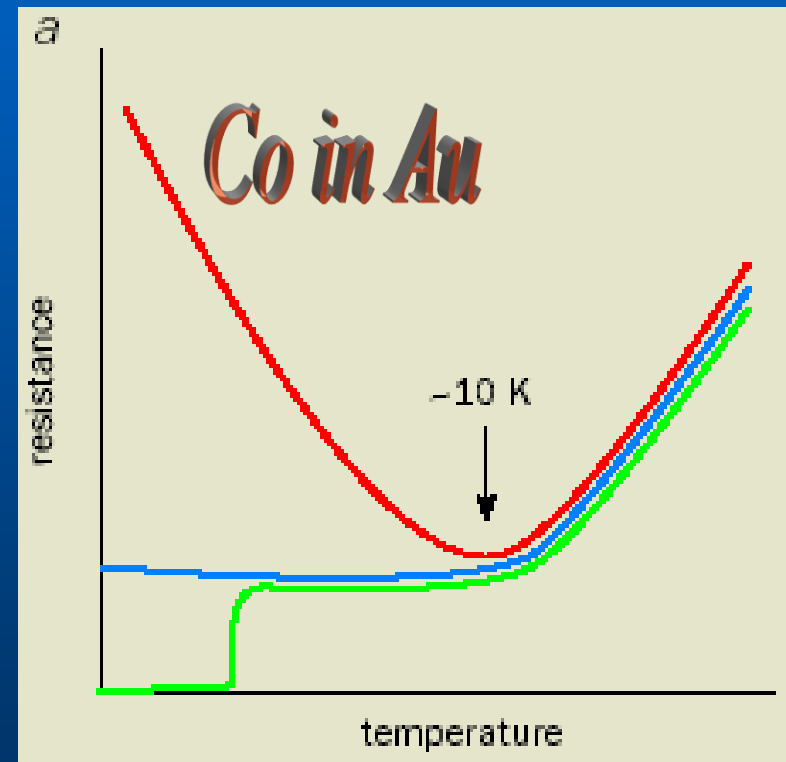
STM image of graphite (E. Andrei et al, Rep. Prog. Phys. 75 (2012) 056501)

You see triangular lattice for graphite and honeycomb lattice for graphene

I. Kondo effect: Many-body physics in metals

Started as a minor problem: Resistivity minimum

- 1933 van den Berg: exp.
- 1964 Jun Kondo: theory

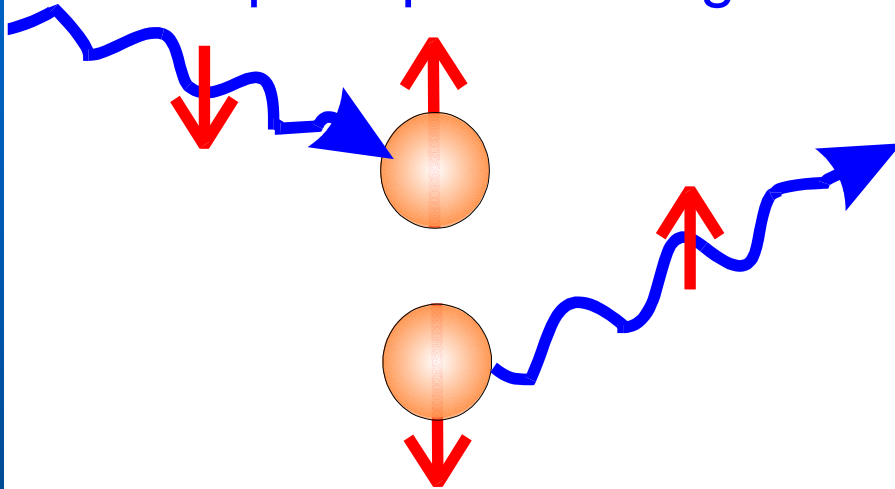


Cu

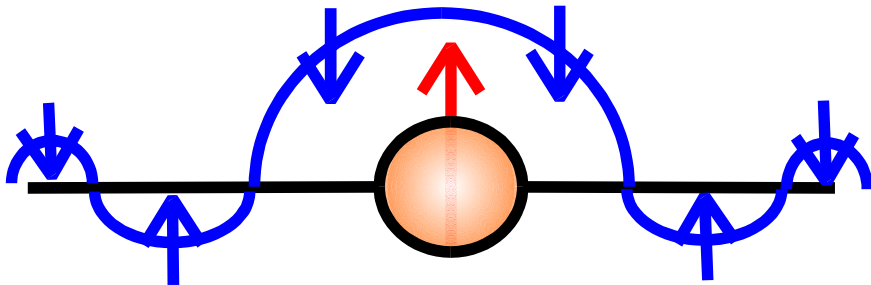
Nb

Kondo effect: theory

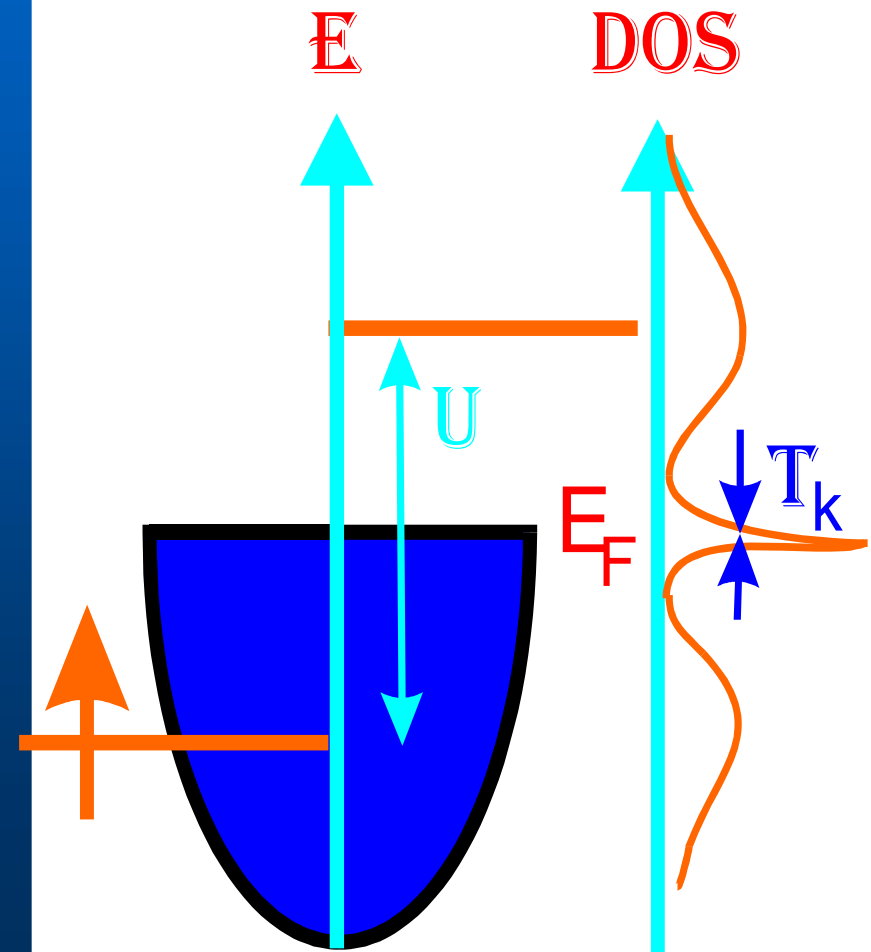
Spin-flip scattering



Kondo-coherence



Kondo-resonance

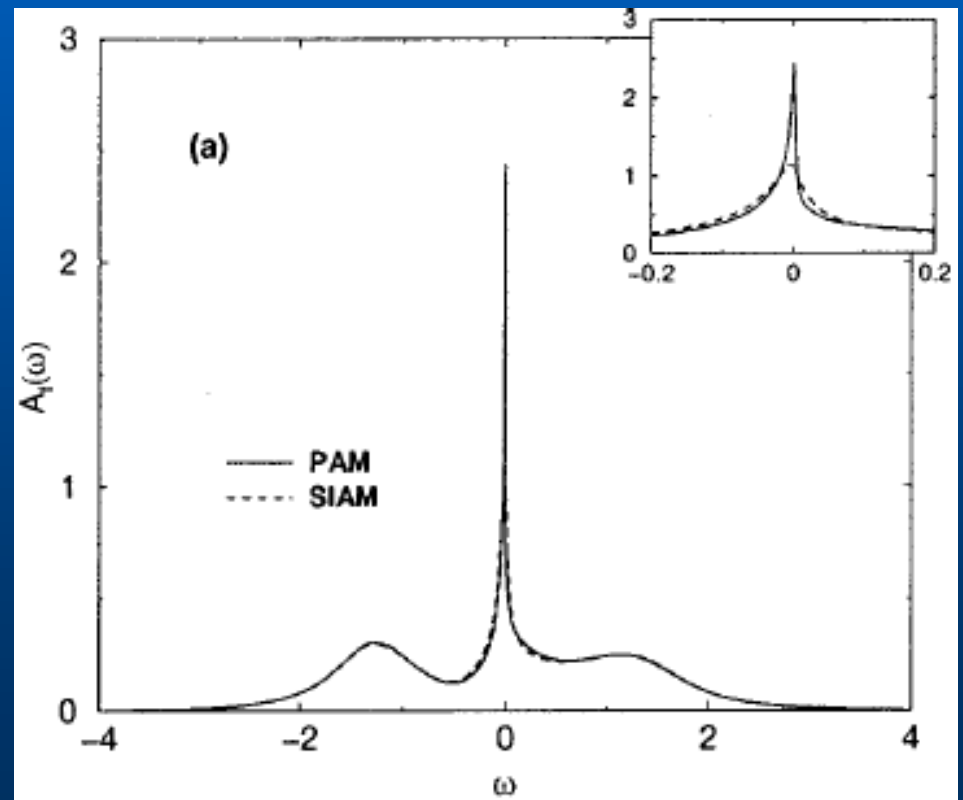


Periodic Anderson Model

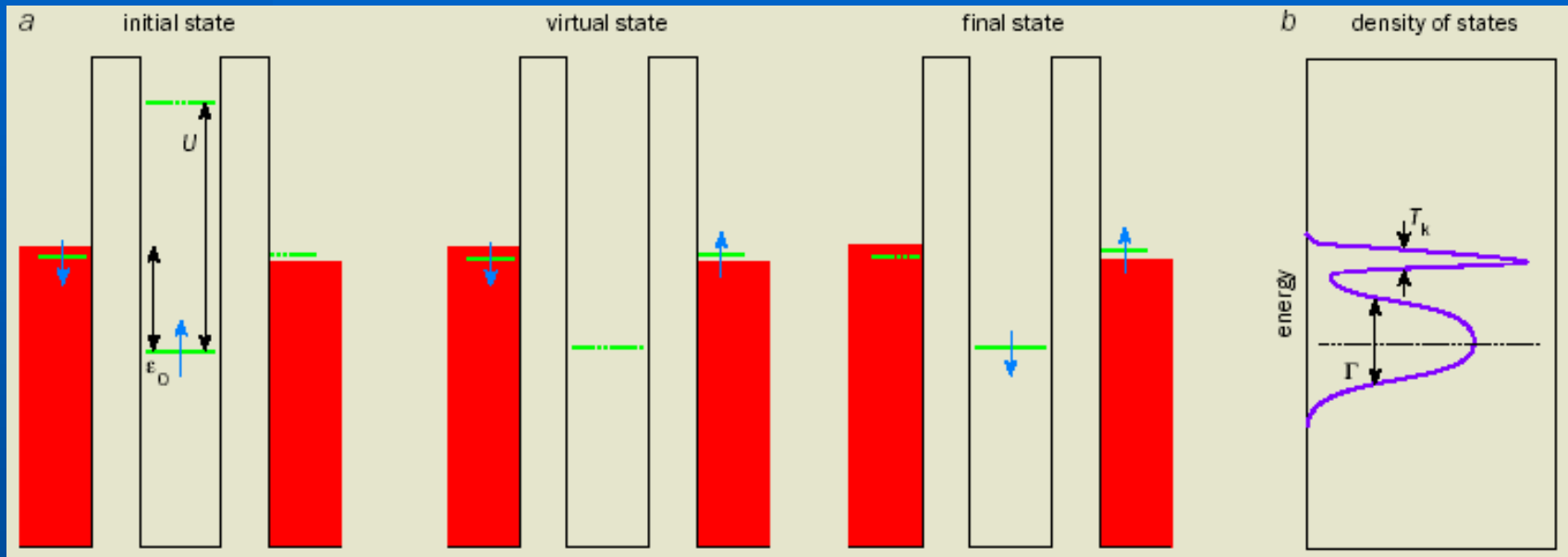
Th. Pruschke, R. Bulla and M. Jarrell, PRB 2000

- PAM vs. SIAM
- Wilson NRG

$$G^{\text{loc}}(z) \int d\epsilon \frac{\rho_0^c(\epsilon)}{z - \epsilon_f - \Sigma^f(z) - \frac{V^2}{z - \epsilon - \epsilon_c}}$$
$$= \frac{1}{z - \epsilon_f - \tilde{\Delta}(z) - \Sigma^f(z)} = G^{\text{SIAM}}(z),$$



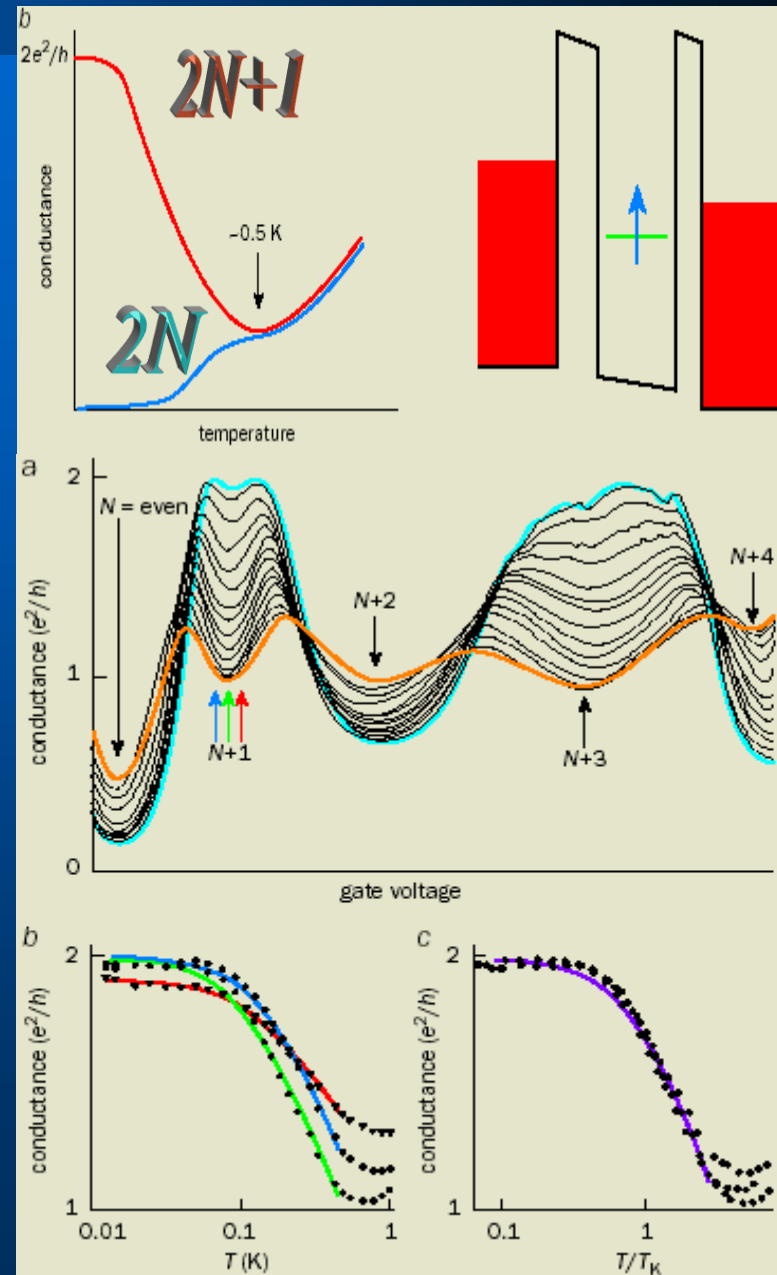
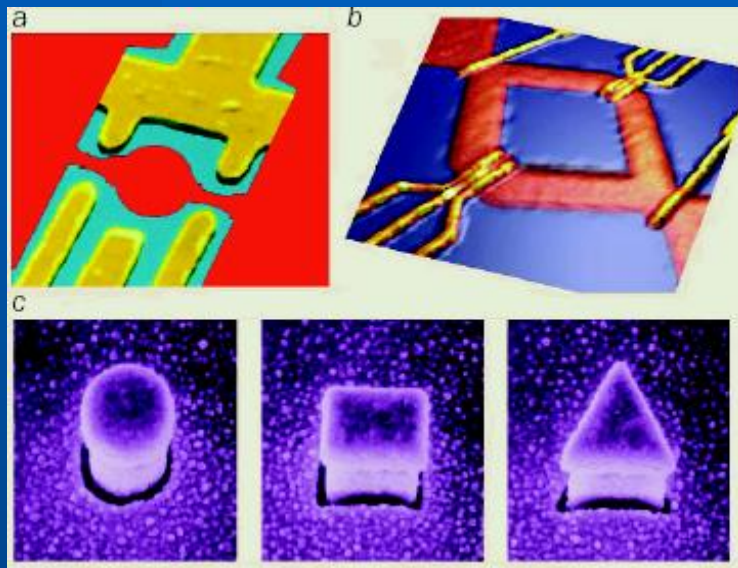
Kondo energy scale



*Kondo temperature
exponentially
depends on parameters:
 T_K can varied from 0.1 K
till 1000 K*

$$T_K = \frac{\sqrt{\Gamma U}}{2} e^{-\frac{\pi \epsilon_0 (\epsilon_0 + U)}{\Gamma U}}$$

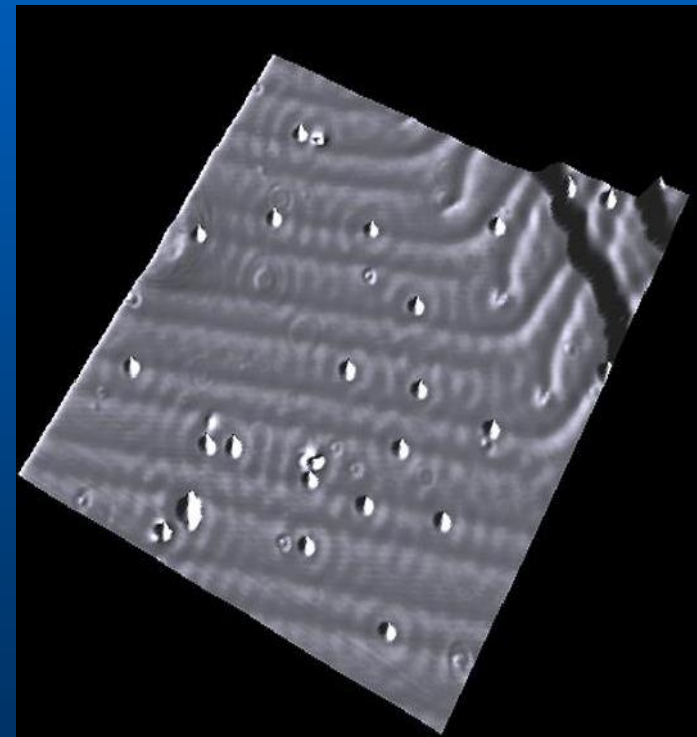
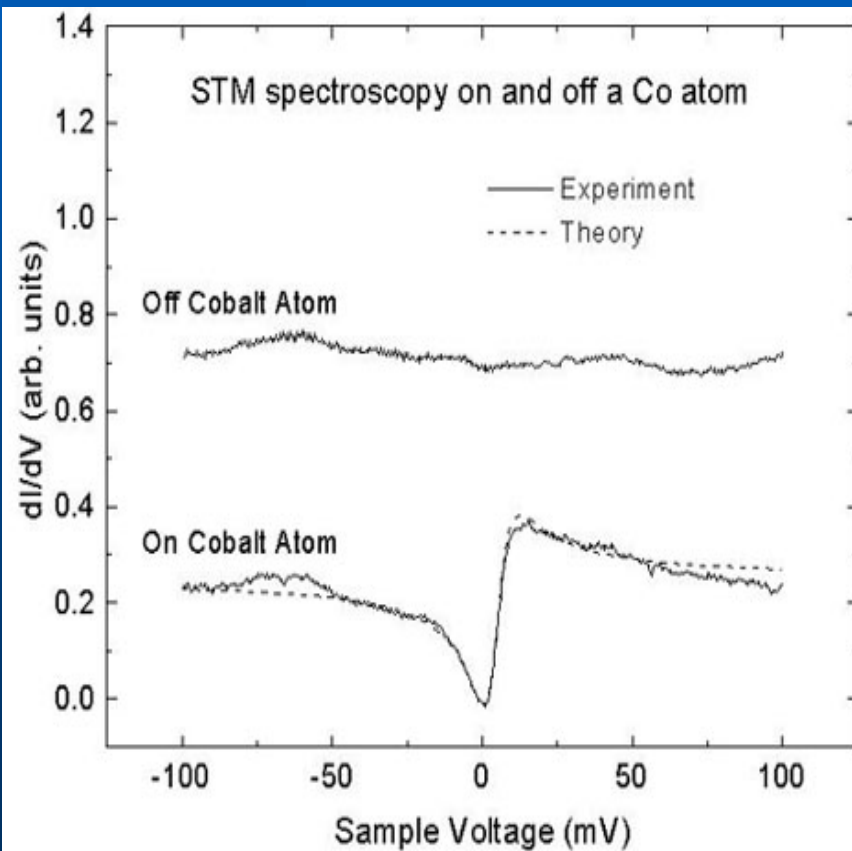
Quantum Dots



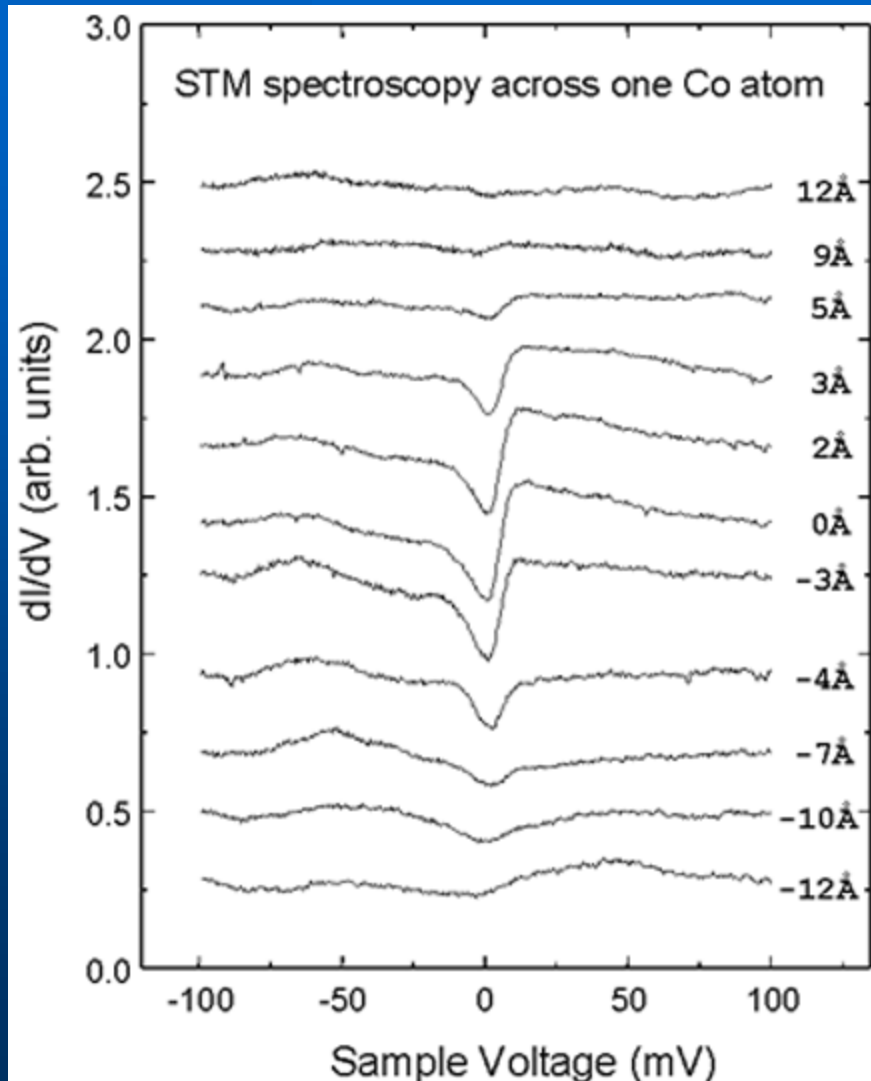
STM: impurity Kondo (M. Crommie)

- Fano STM resonance

- Single Co atom on Au



Kondo coherence: Co atom on Au



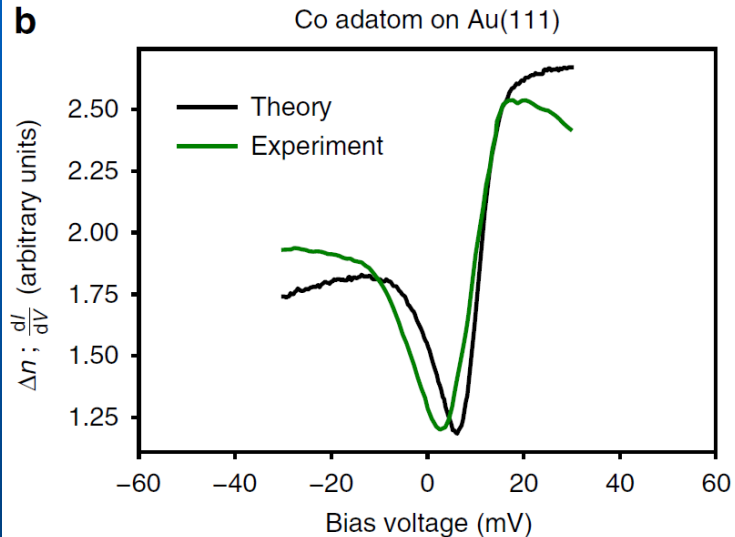
- M. Crommie:
- The Kondo resonance is fall off over a distance of about 10 Å

Recent criticism of interpretation

A new view on the origin of zero-bias anomalies of Co atoms atop noble metal surfaces

Juba Bouaziz¹, Filipe Souza Mendes Guimarães¹ & Samir Lounis¹

NATURE COMMUNICATIONS | (2020)11:6112 |



Still many-body physics, still spin flip processes but perturbative; the key role of spin-orbit coupling and magnetic anisotropy

No real contraction I believe since the unified description is possible

Spins are not free but still some remnants of Kondo physics survive

PHYSICAL REVIEW B

VOLUME 56, NUMBER 13

1 OCTOBER 1997-I

Scaling picture of magnetism formation in the anomalous f -electron systems: Interplay of the Kondo effect and spin dynamics

V. Yu. Irkhin and M. I. Katsnelson*

Institute of Metal Physics, 620219 Ekaterinburg, Russia

(Received 27 December 1996; revised manuscript received 15 May 1997)

PHYSICAL REVIEW B

VOLUME 59, NUMBER 14

1 APRIL 1999-II

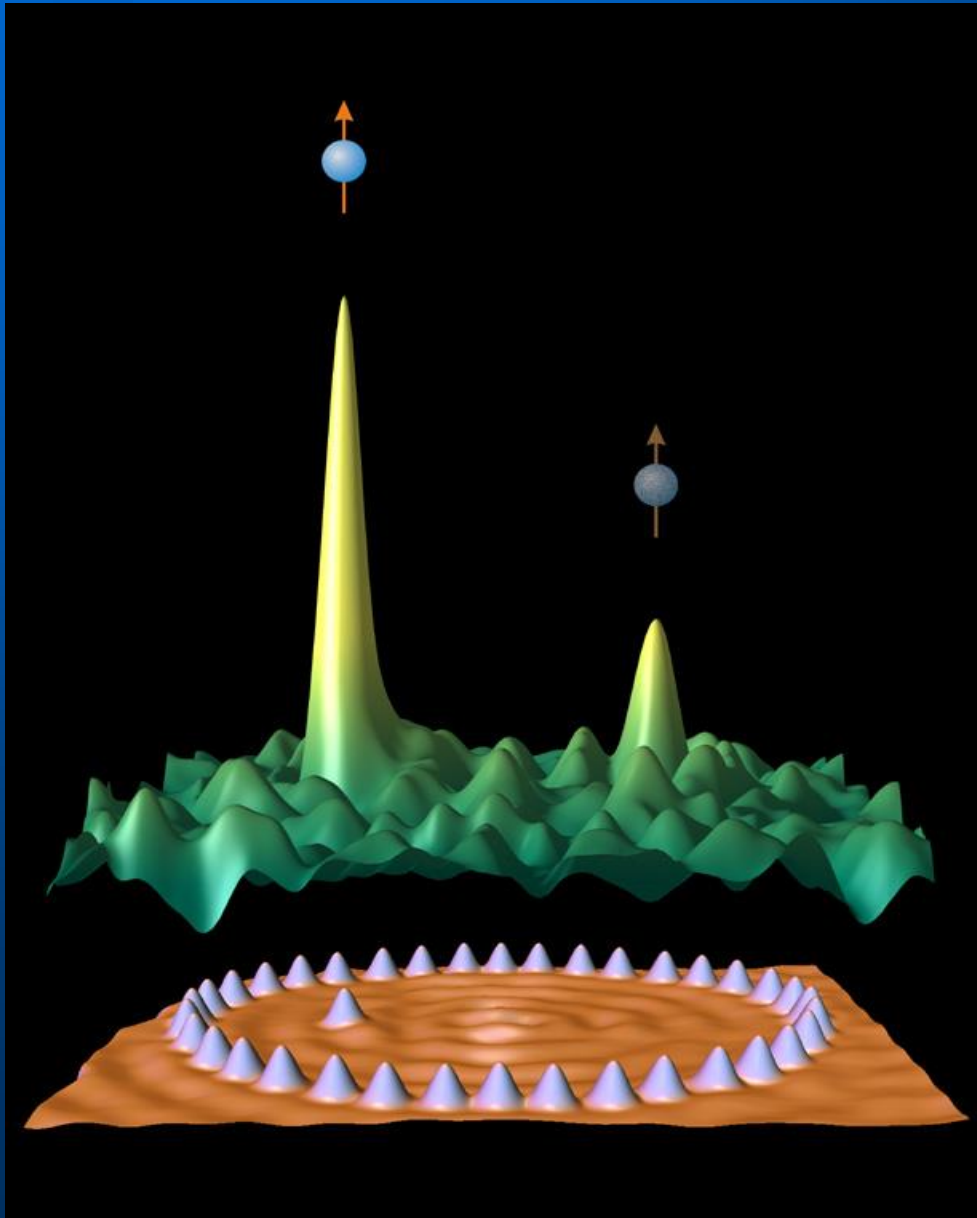
Scaling theory of magnetic ordering in the Kondo lattices with anisotropic exchange interactions

V. Yu. Irkhin* and M. I. Katsnelson

Institute of Metal Physics, 620219 Ekaterinburg, Russia

(Received 26 May 1998; revised manuscript received 5 October 1998)

Quantum mirage (D. Eigler, IBM)



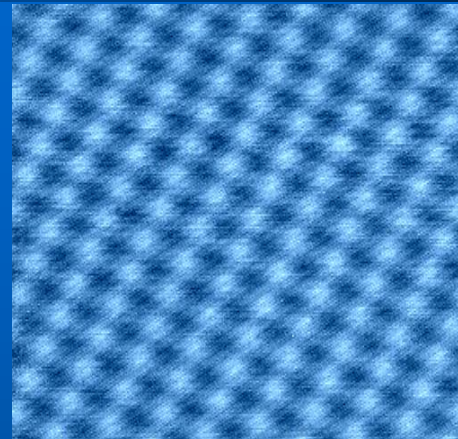
- 48 Co atoms on Cu(111) confined in the quantum corrals plus one extra Co atom

Orbital Kondo resonance?

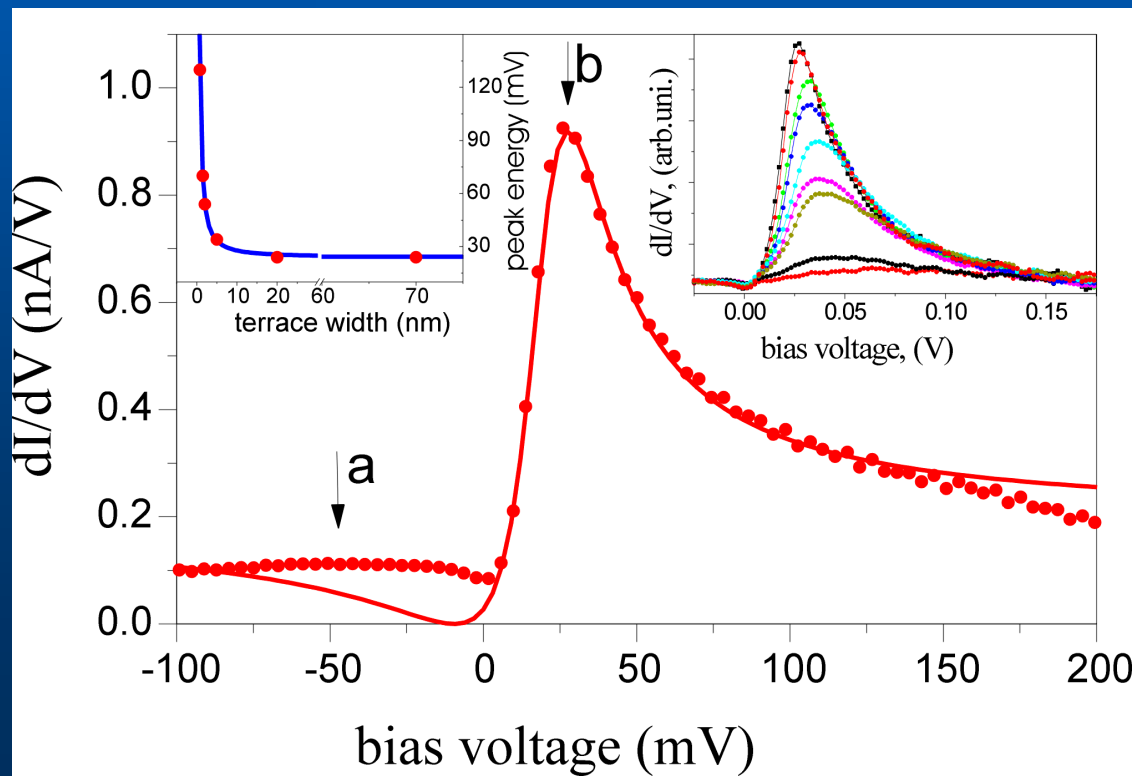
Real-space imaging of an orbital Kondo resonance on the Cr(001) surface

O. Yu. Kolesnychenko, R. de Kort, M. I. Katsnelson, A. I. Lichtenstein & H. van Kempen

NATURE | VOL 415 | 31 JANUARY 2002



Atomically
clean
surface

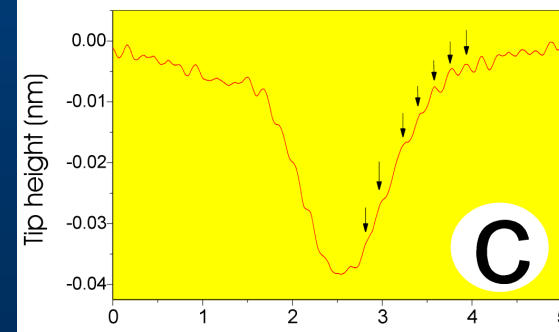
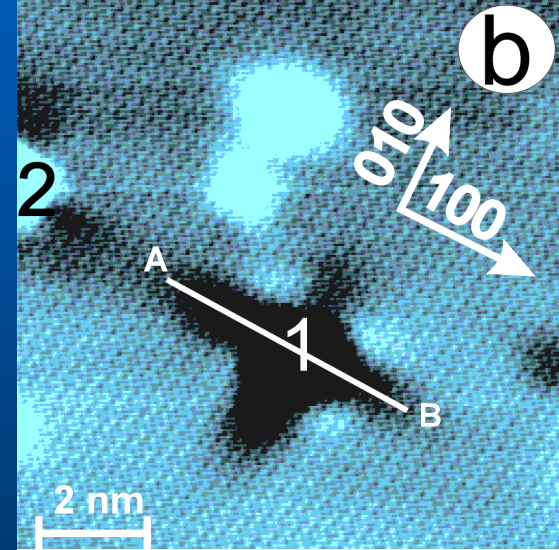
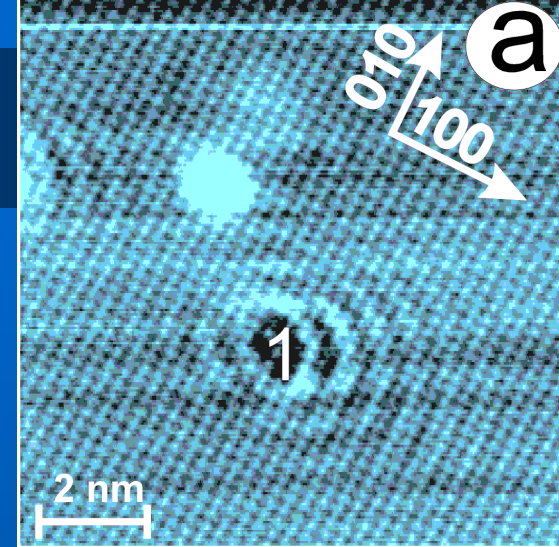
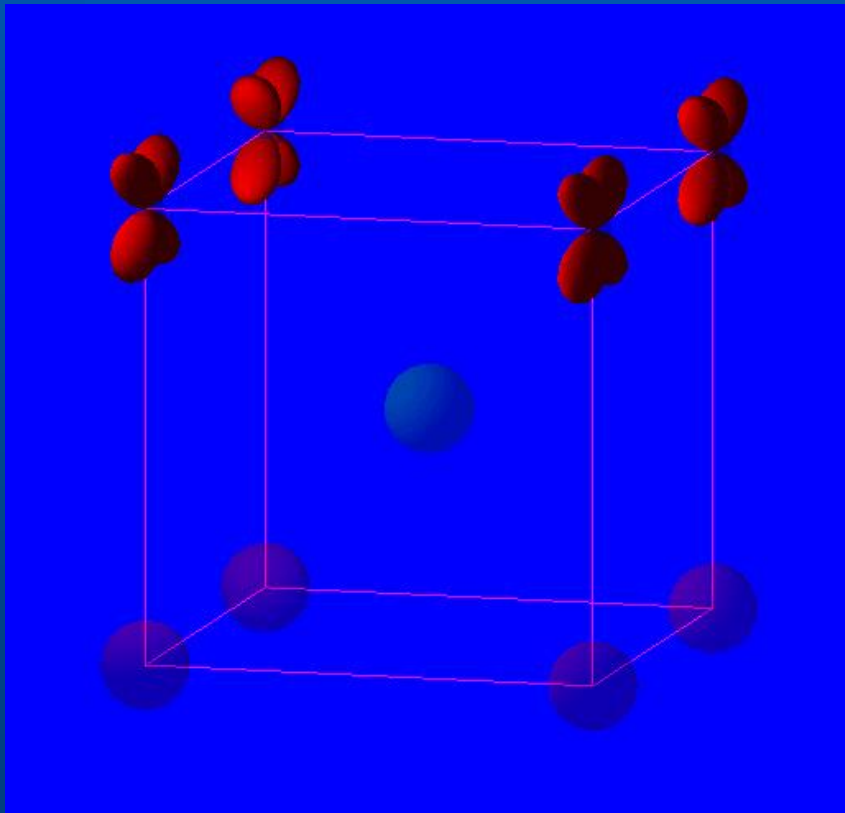


Disappeared at high temperature

Suppressed near terrace edge (breaks degeneracy between xy and xz states)

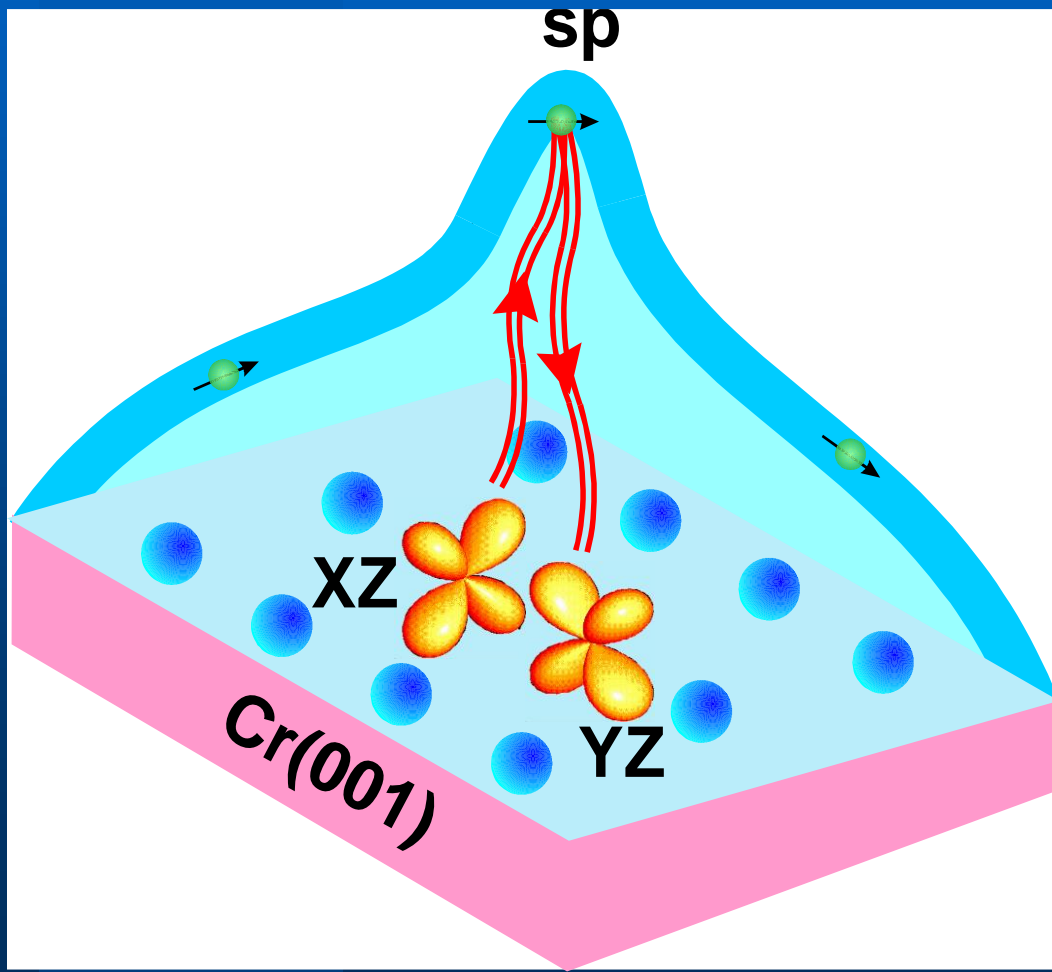
STM: orbital character

- Friedel oscillations away from peak
- Two degenerate surface states at the resonance: xz and yz



Orbital Kondo Effect

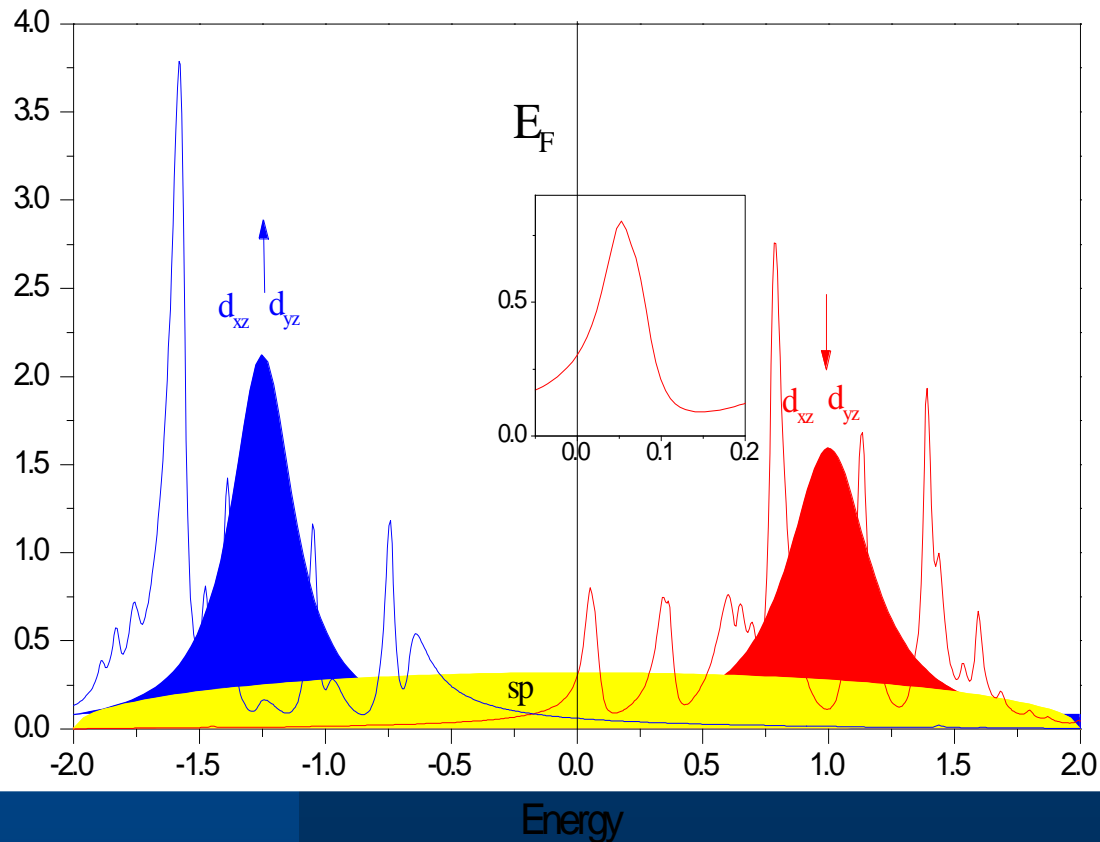
$$H = \sum_{km\sigma} \left[E_0^\sigma f_{km\sigma}^+ f_{km\sigma} + \varepsilon_{km\sigma} c_{km\sigma}^+ c_{km\sigma} + V^\sigma (c_{km\sigma}^+ f_{km\sigma} + f_{km\sigma}^+ c_{km\sigma}) \right] + \frac{1}{2} \sum_{i,m,m',\sigma,\sigma'} U_{m,m'}^{\sigma,\sigma'} n_{im\sigma} n_{im'\sigma'}$$



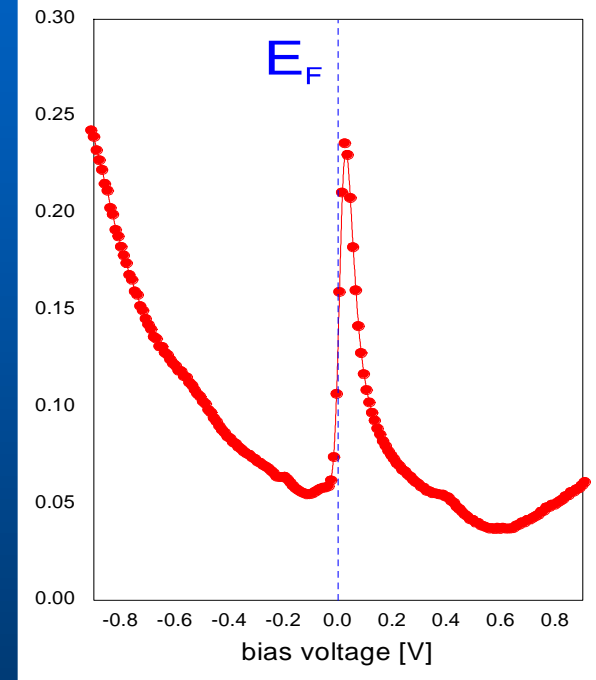
- Periodic degenerate Anderson model
- Position of d-levels from FM-surface Cr(001) calculation
- $U=1.2$ eV $J=0.4$ eV
- Two-orbital DMFT with ED-method

Formation of orbital Kondo resonance

degenerate PAM in DMFT



STM on Cr(001)



- STM-Kondo peak
- Protected xz - yz degeneracy on Cr(001) surface

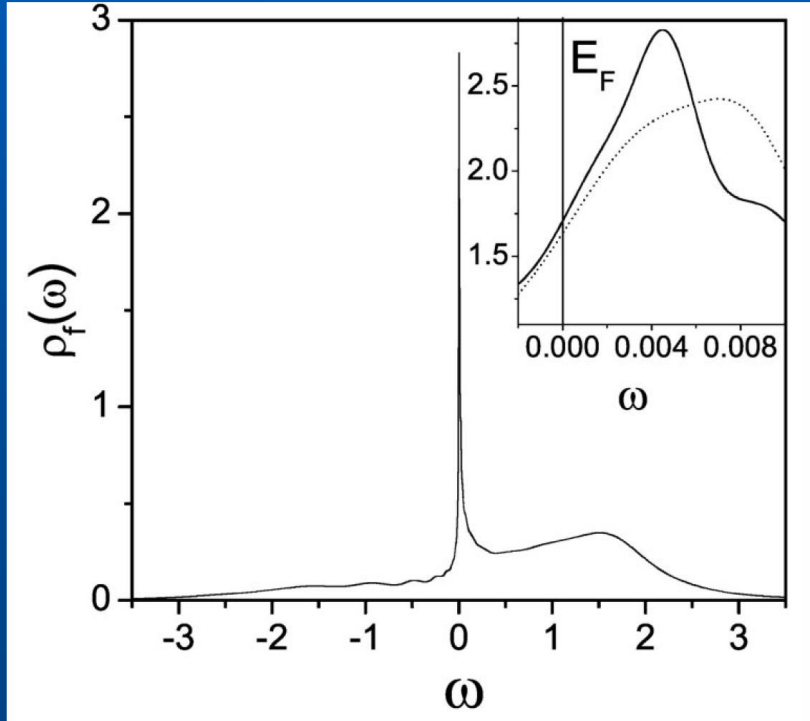
Kondo resonance for orbitally degenerate system

Friedel sum rule: the resonance should be shifted from E_F

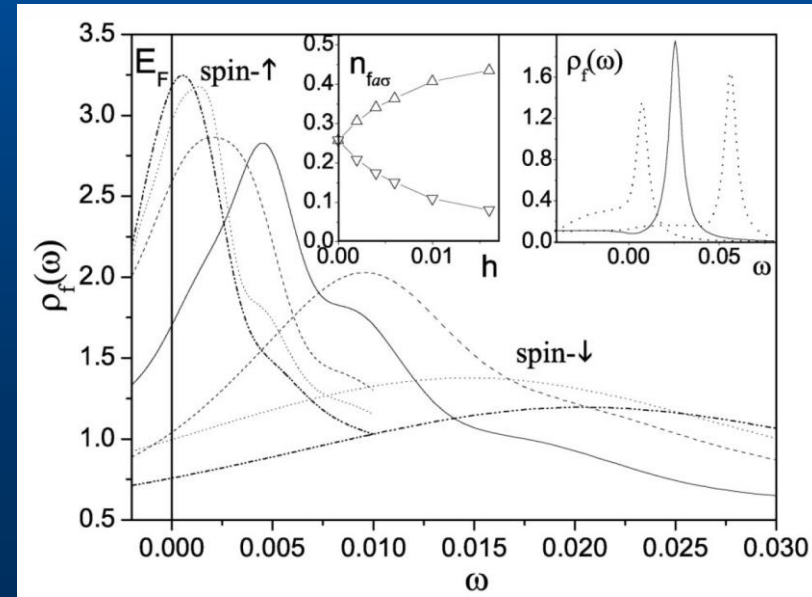
$$2(2l + 1)\eta_l/\pi = n_f$$

$$\rho_f(0) = \frac{1}{\pi\Gamma} \sin^2\left(\frac{\pi n_f}{N}\right)$$

Double degenerate Anderson model, quarter filled
NRG results
(Zhuravlev, Irkhin, MIK, Lichtenstein, PRL 2004)



Effect of magnetic field on the Kondo resonance



Further studies

PHYSICAL REVIEW B 72, 085453 (2005)

Temperature-dependent scanning tunneling spectroscopy of Cr(001): Orbital Kondo resonance versus surface state

T. Hänke, M. Bode,* S. Krause, L. Berbil-Bautista, and R. Wiesendanger

There is pure band surface state of d_z^2 character but...

Huge T -dependence

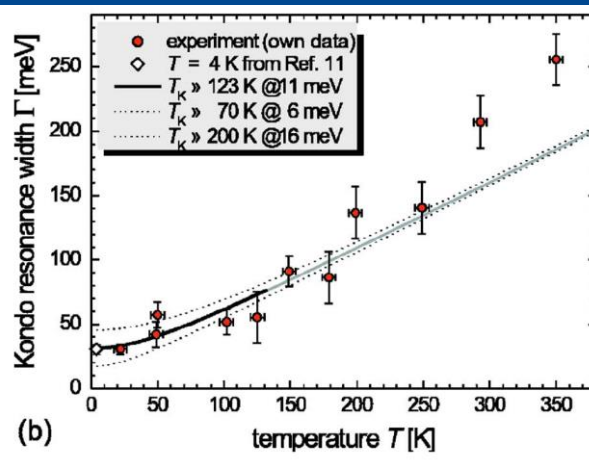
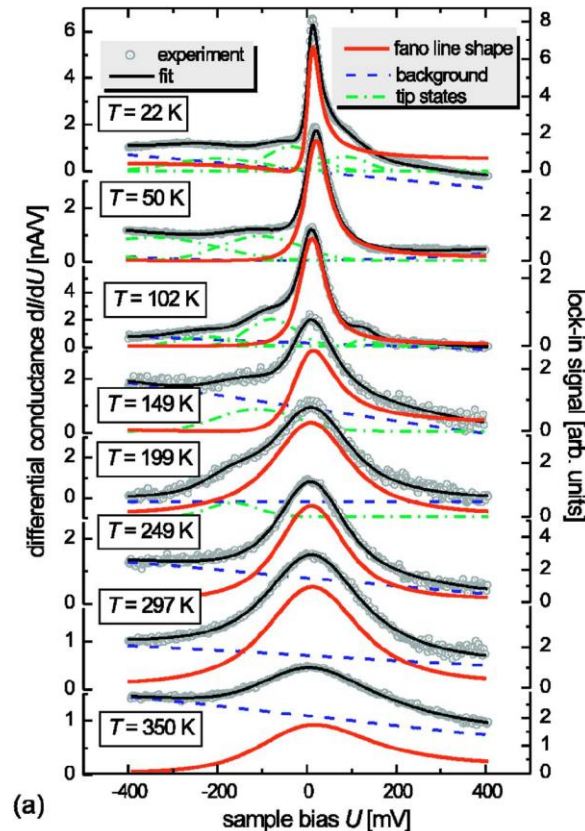
Low- T data:
good agreement
with us

Alternative explanation:
polaronic effect?!

Strong spin-orbit
coupling is required

$$\lambda = 1.53 \pm 0.40$$

How real is it?



Checking polaronic hypothesis

PHYSICAL REVIEW B **97**, 165438 (2018)

Ab initio study of the electron-phonon coupling at the Cr(001) surface

L. Peters,^{1,*} A. N. Rudenko,^{2,3,1} and M. I. Katsnelson^{1,3}

T-dependence of peak width

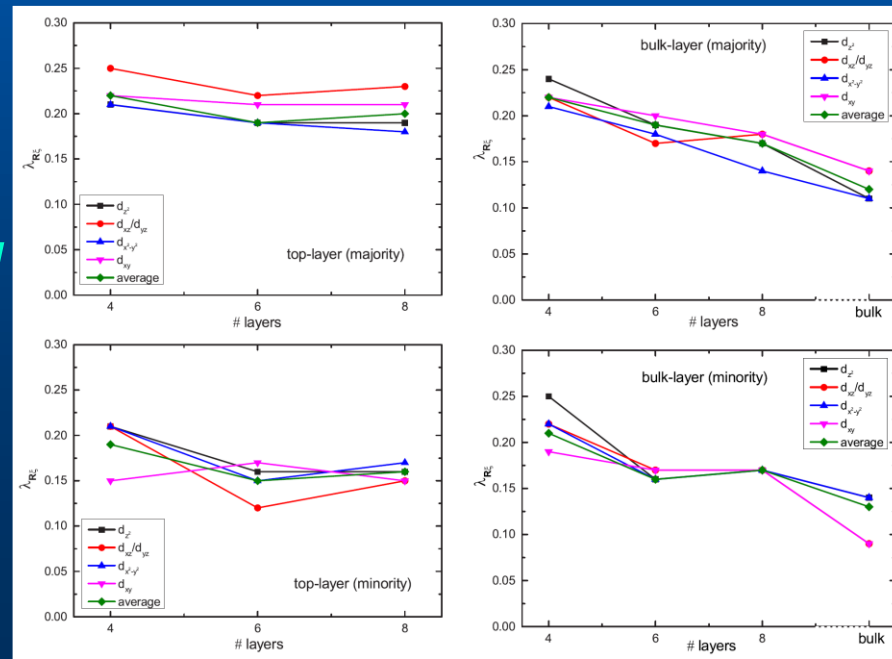
$$\Gamma_{e-ph}(T) = \Gamma_{ee} + \lambda_{\text{sur}} \frac{2\pi}{\omega_D^2} \int_0^{\omega_D} dE' E'^2 [1 - f(E_0 - E') + 2n(E') + f(E_0 + E')]. \quad (10)$$

$f(E)$ the Fermi distribution, and $n(E)$ the Bose-Einstein distribution

We need at least

$$\lambda_{\text{sur}} = 0.77 \pm 0.16$$

Real values of lambda are several times too weak to explain observed temperature dependence



First principles DFT+DMFT calculations

PHYSICAL REVIEW B **93**, 195115 (2016)

Many-body effects on Cr(001) surfaces: An LDA+DMFT study

M. Schüler,^{1,2,*} S. Barthel,^{1,2} M. Karolak,³ A. I. Poteryaev,^{4,5} A. I. Lichtenstein,^{6,7} M. I. Katsnelson,^{8,7} G. Sangiovanni,³ and T. O. Wehling^{1,2}

PHYSICAL REVIEW B **96**, 245137 (2017)

Origin of the quasiparticle peak in the spectral density of Cr(001) surfaces

L. Peters,^{1,*} D. Jacob,² M. Karolak,³ A. I. Lichtenstein,⁴ and M. I. Katsnelson¹

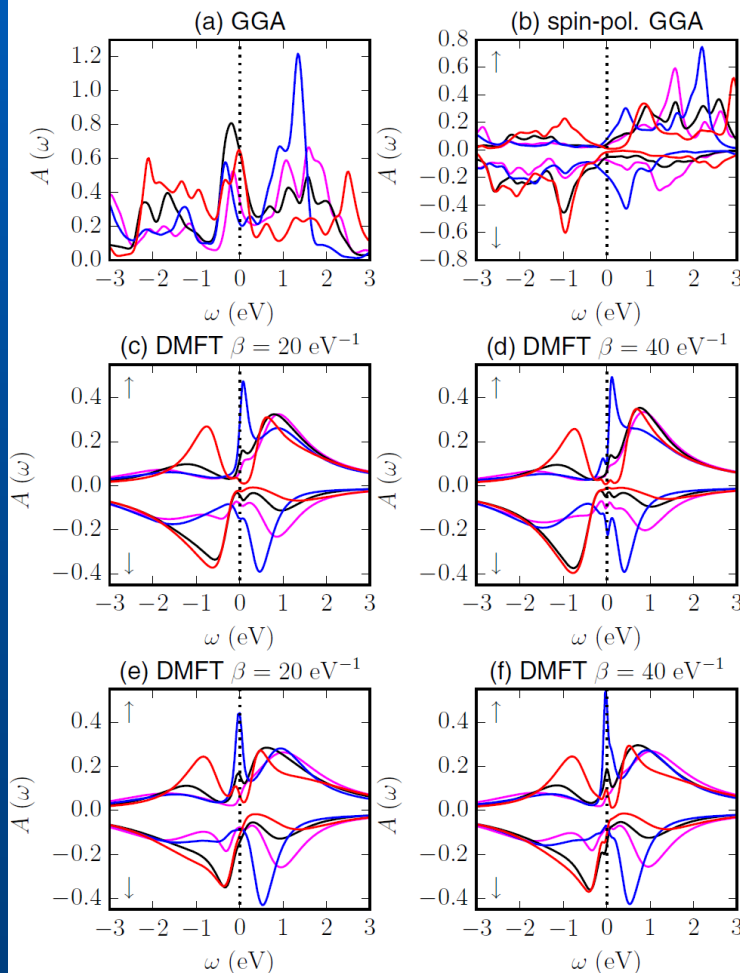


FIG. 3. Orbitally resolved local density of states of the surface atom from (a) GGA, (b) spin-polarized GGA, and LDA+DMFT simulations at different double-counting energies and temperatures, (c) $\beta = 20 \text{ eV}^{-1}$ and (d) $\beta = 40 \text{ eV}^{-1}$ at $E_{\text{dc}} \approx 13.5 \text{ eV}$ (trace double counting), and (e) $\beta = 20 \text{ eV}^{-1}$ and (f) $\beta = 40 \text{ eV}^{-1}$ at $E_{\text{dc}} \approx 12.2 \text{ eV}$.

- Correlation effects are crucially important;
- d_z^2 peak is dominant near E_F at relatively large energy scales;
- energy resolution of the existing solvers is not sufficient to describe *ab initio* Kondo orbital physics

II. Graphene

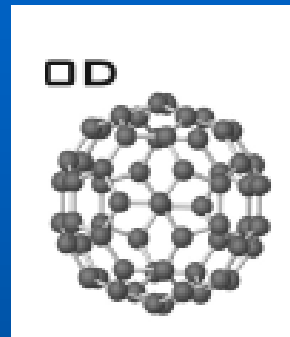
Allotropes of carbon



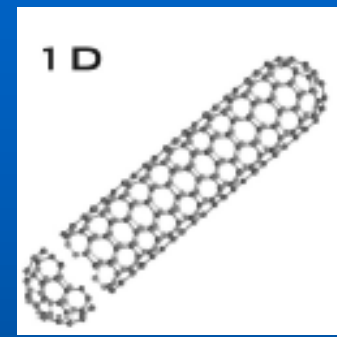
Diamond



Graphite



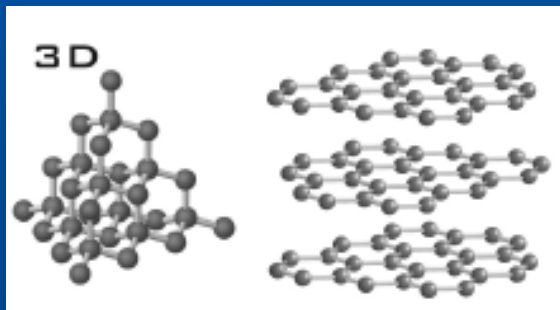
Fullerenes



Nanotubes

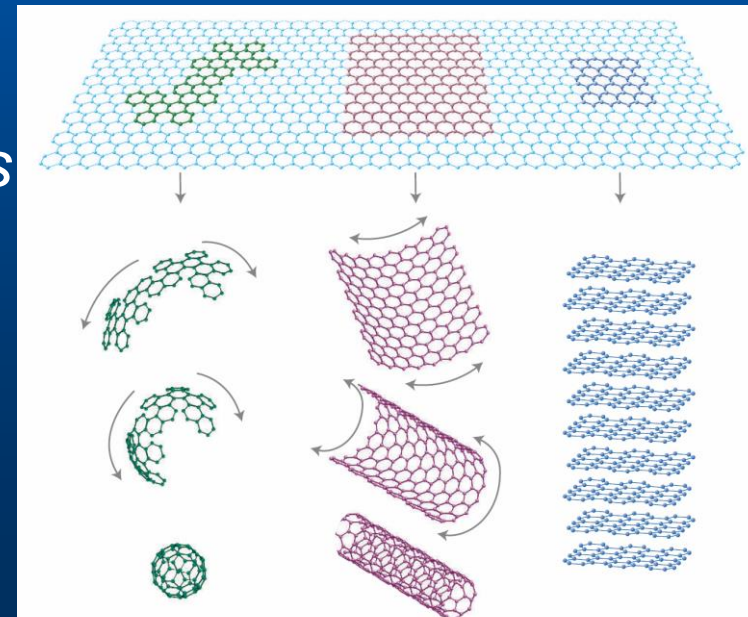


Graphene



Mother of all
graphitic forms

Honeycomb lattice



Massless Dirac fermions

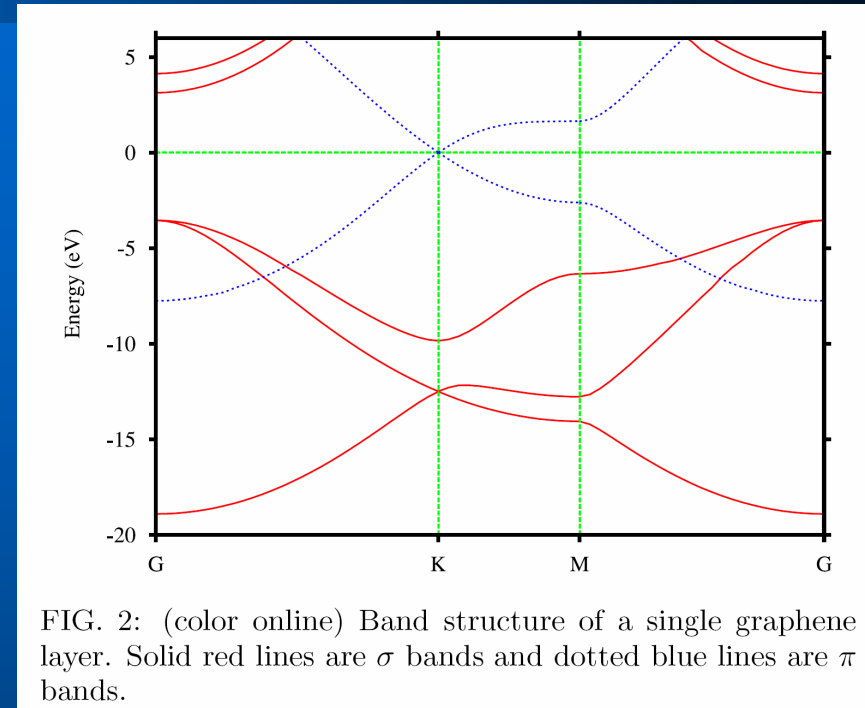
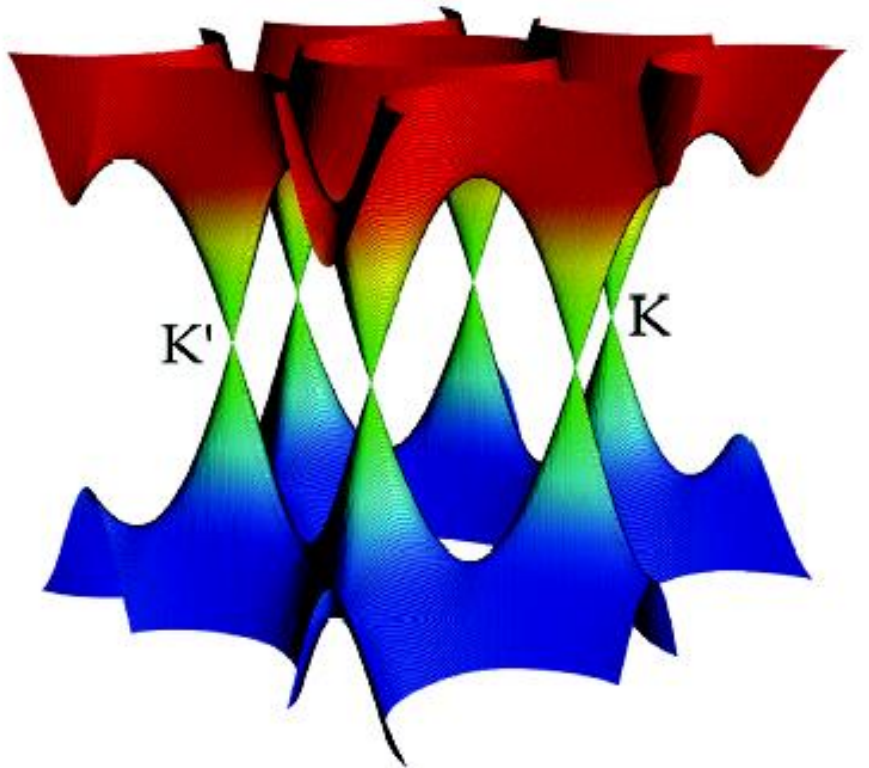
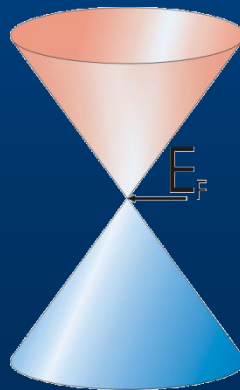


FIG. 2: (color online) Band structure of a single graphene layer. Solid red lines are σ bands and dotted blue lines are π bands.

sp^2 hybridization, π bands crossing the neutrality point

Massless relativistic particles (light cones)

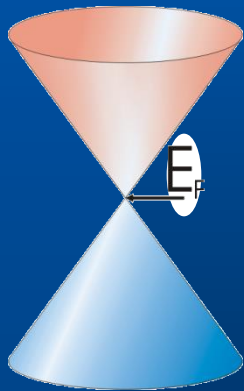


Neglecting intervalley scattering: massless Dirac fermions

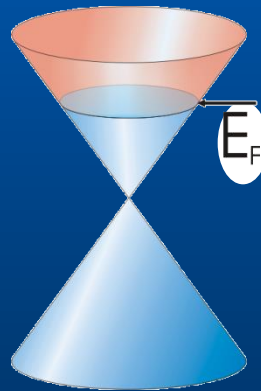
Symmetry protected (T and I)

Massless Dirac fermions II

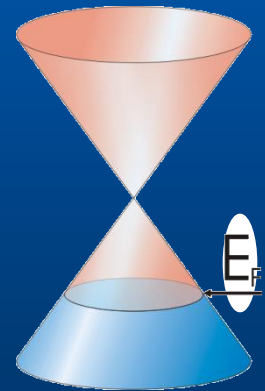
Spectrum near K (K') points is linear.
Conical cross-points: provided by symmetry and thus robust property



Undoped



Electron



Hole

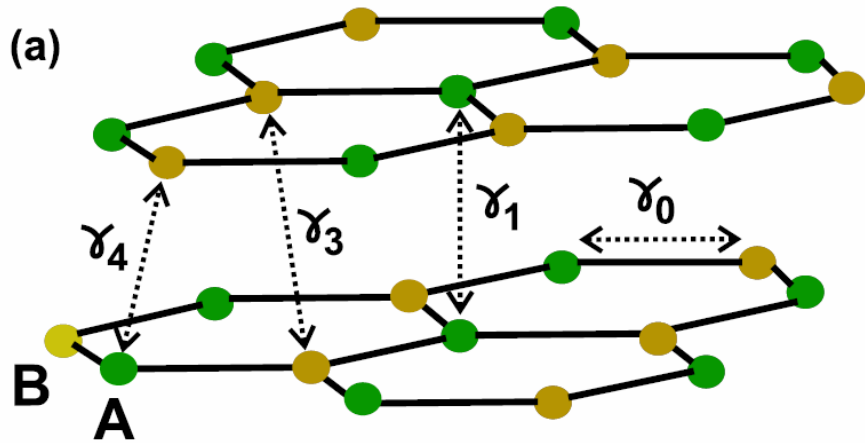
Massless Dirac fermions III

*If Umklapp-processes K - K' are neglected:
2D Dirac massless fermions with the Hamiltonian*

$$H = -i\hbar c^* \begin{pmatrix} 0 & \frac{\partial}{\partial x} - i \frac{\partial}{\partial y} \\ \frac{\partial}{\partial x} + i \frac{\partial}{\partial y} & 0 \end{pmatrix} \quad \hbar c^* = \frac{\sqrt{3}}{2} \gamma_0 a$$

*“Spin indices” label sublattices A and B
rather than real spin (pseudospin)*

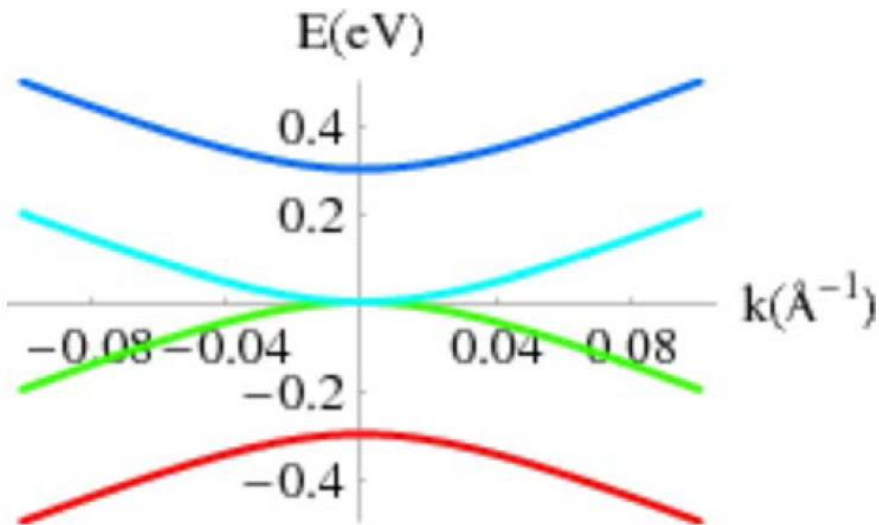
Bilayer graphene – TB description



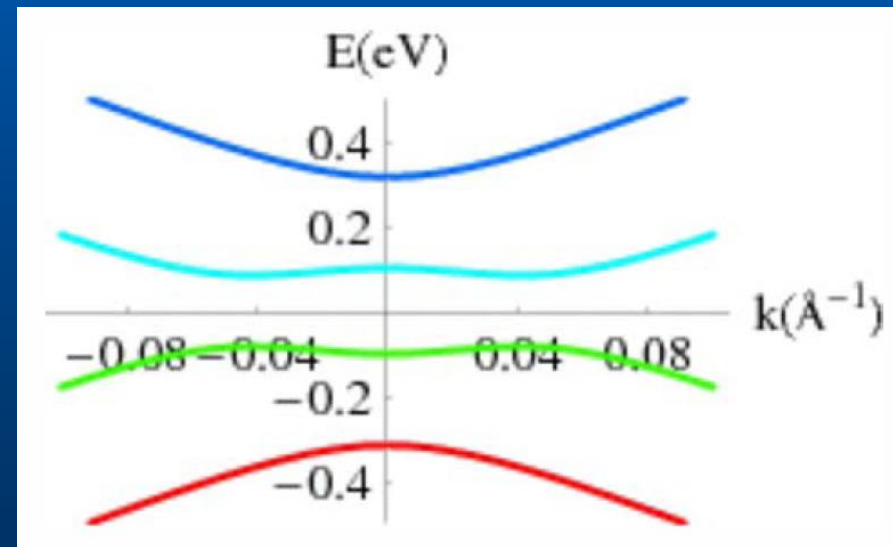
$$H = \begin{pmatrix} 0 & -(p_x - ip_y)^2/2m \\ -(p_x + ip_y)^2/2m & 0 \end{pmatrix}$$

$$m^* \approx 0.028m_e$$

(neglecting γ_3)



Gapless, parabolic



Electric field perp. layers

Bilayer graphene II

Trigonal warping, many-body effects and spectrum reconstruction at small energies

Single-particle Hamiltonian:

$$\hat{H}_K = \begin{pmatrix} 0 & \frac{(\hat{p}_x - i\hat{p}_y)^2}{2m^*} + \frac{3\gamma_3 a}{\hbar} (\hat{p}_x + i\hat{p}_y) \\ \frac{(\hat{p}_x + i\hat{p}_y)^2}{2m^*} + \frac{3\gamma_3 a}{\hbar} (\hat{p}_x - i\hat{p}_y) & 0 \end{pmatrix}$$



Interaction-Driven Spectrum Reconstruction in Bilayer Graphene

A. S. Mayorov,¹ D. C. Elias,¹ M. Mucha-Kruczynski,² R. V. Gorbachev,³ T. Tudorovskiy,⁴
A. Zhukov,³ S. V. Morozov,⁵ M. I. Katsnelson,⁴ V. I. Fal'ko,² A. K. Geim,³ K. S. Novoselov^{1*}

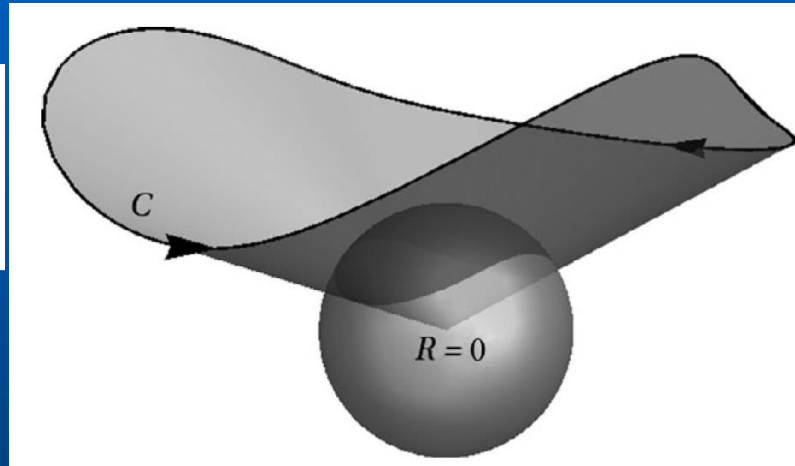
12 AUGUST 2011 VOL 333 SCIENCE

Berry phase and winding number in graphene

For two-band Hamiltonian

$$\hat{H}_{\text{eff}} = \frac{1}{2} \vec{R}(\vec{k}) \vec{\sigma}$$

$$\gamma_{\pm}(C) = \mp \frac{1}{2} \Omega(C)$$



Single-layer graphene

solid angle is 2π , so the Berry phase is $\gamma_{+} = \mp \pi$

Bilayer graphene $\gamma = 2\pi$

Rhombohedral N-layer $\gamma = N\pi$

Berry phase and winding number in graphene II

PHYSICAL REVIEW B **75**, 155424 (2007)

Existence and topological stability of Fermi points in multilayered graphene

J. L. Mañes,¹ F. Guinea,² and María A. H. Vozmediano³

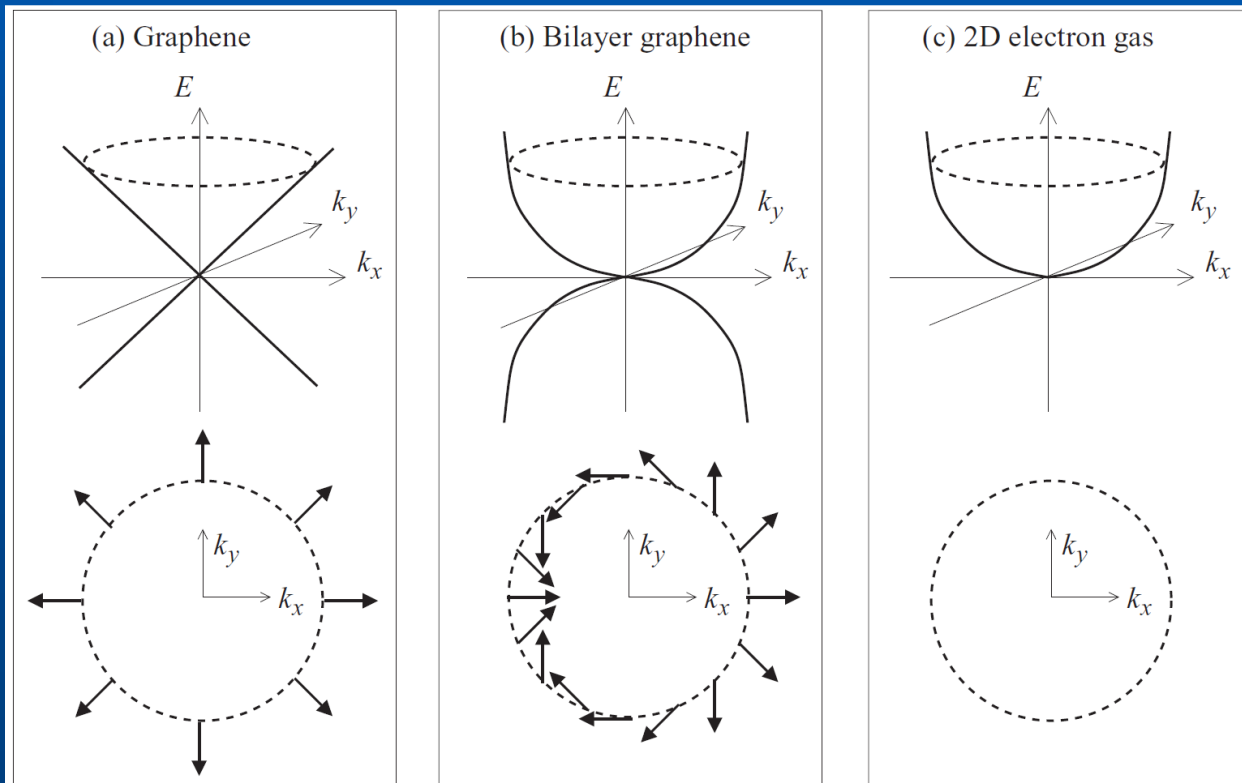
PHYSICAL REVIEW B **84**, 205440 (2011)



Berry phase and pseudospin winding number in bilayer graphene

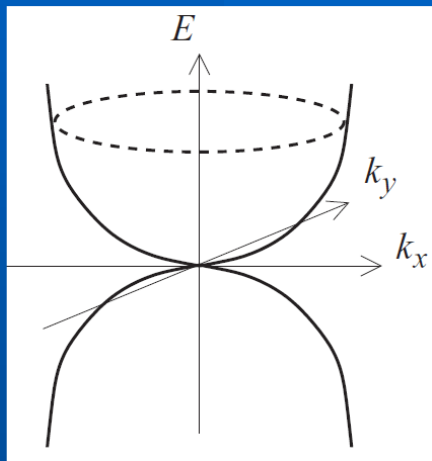
Cheol-Hwan Park^{1,2,*} and Nicola Marzari^{2,3}

More accurate language: Winding number (what happens with pseudospin vector at full rotation)



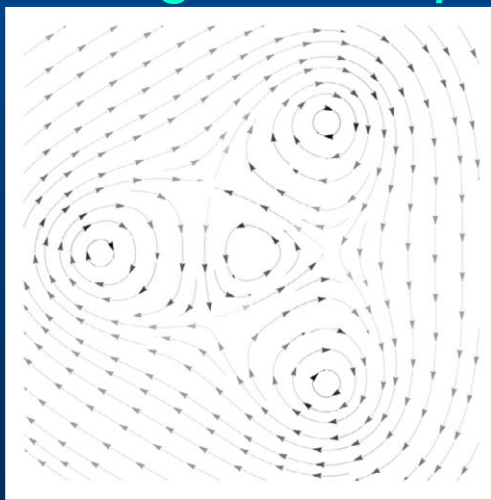
Berry phase and winding number in graphene III

In bilayer graphene winding number is topologically protected



Without trigonal warping With trigonal warping With nematic order

In all cases $N=2$



Distribution of Berry
vector potential:
 $1 + 1 + 1 - 1 = 2$

Berry phase and winding number in graphene IV

Semiclassical quantization condition in magnetic field

$$S(E_n) = \frac{2\pi |e| B}{\hbar c} \left(n + \frac{1}{2} - \frac{\gamma}{2\pi} \right)$$

(n integer, including zero)

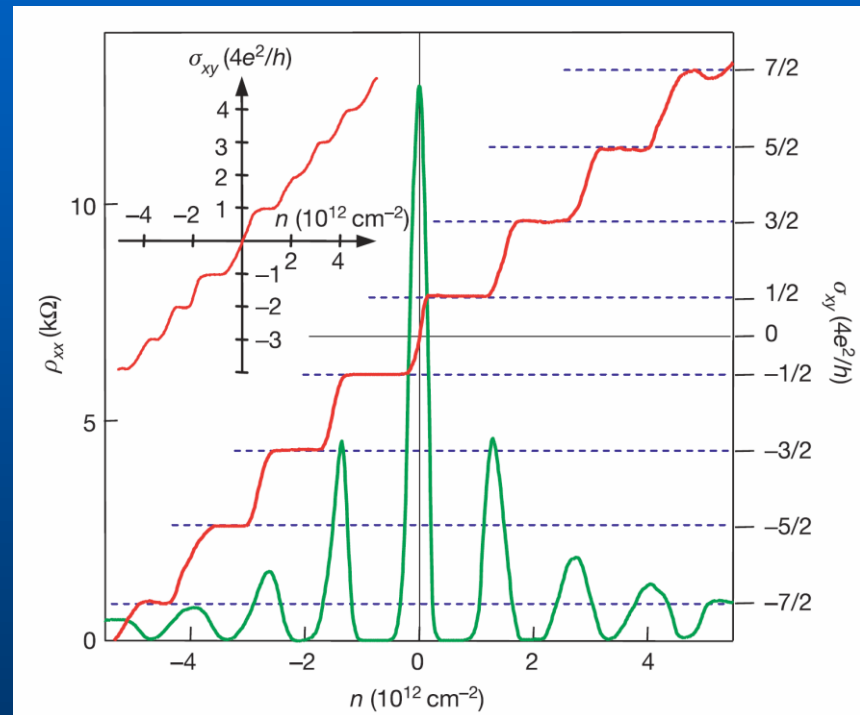
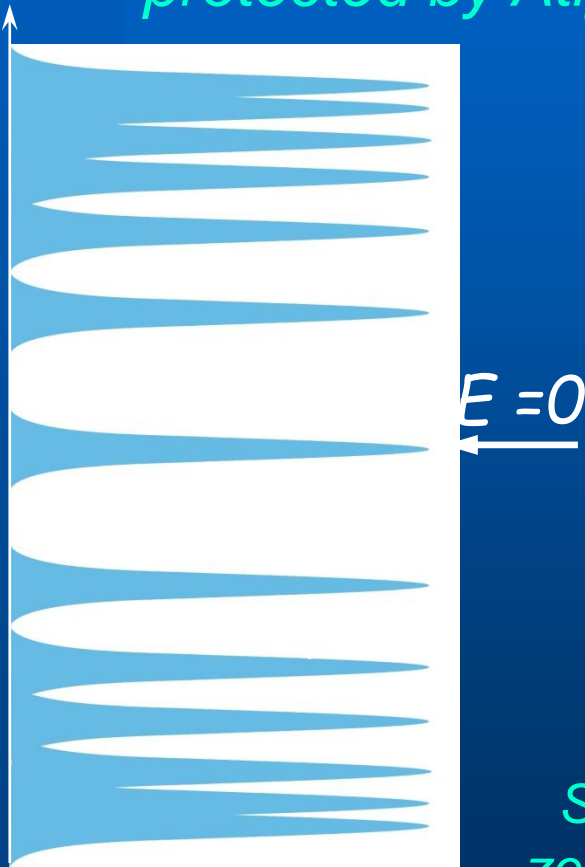
For

$$\gamma = \pi$$

$$S(E_n) = \frac{2\pi |e| B}{\hbar c} n$$

Berry phase and winding number in graphene V

Consequences: zero-energy Landau level (topologically protected by Atiyah-Singer index theorem)



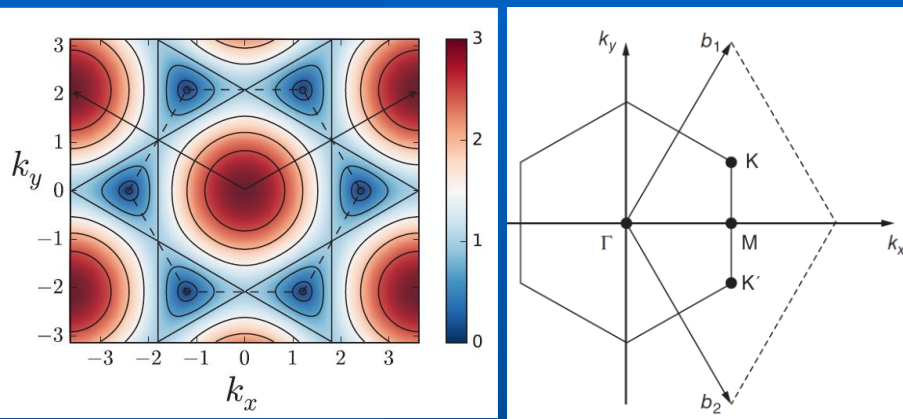
Single-layer: half-integer quantization since zero-energy Landau level is equally shared by electrons and holes (Novoselov et al 2005, Zhang et al 2005)

Manifestations of Berry phase in STM

PHYSICAL REVIEW B **93**, 035413 (2016)

Friedel oscillations at the surfaces of rhombohedral N -layer graphene

C. Dutreix and M. I. Katsnelson



Intervalley transitions are crucially important

$$\mathbf{K}_{mn}^{\xi} = \xi \frac{\mathbf{b}_1 - \mathbf{b}_2}{3} + m\mathbf{b}_1 + n\mathbf{b}_2$$

$$\xi = \pm 1 \text{ for } K \text{ and } K'$$

Dirac wave functions

$$|\Psi_{\pm}(\mathbf{K}_{mn}^{\xi} + \mathbf{q})\rangle \simeq \frac{1}{\sqrt{2}} \begin{pmatrix} 1 \\ \mp \xi e^{-i\mathbf{K}_{mn}^{\xi} \cdot \mathbf{d}_3} e^{-i\theta^{\xi}(\mathbf{q})} \end{pmatrix} \quad \theta_{mn}^{\xi}(\mathbf{q}) = \mathbf{K}_{mn}^{\xi} \cdot \mathbf{d}_3 + \theta^{\xi}(\mathbf{q}) \quad \mathbf{d}_3 = (0, -1)$$

$\theta^{\xi}(\mathbf{q}) = \xi \theta_{\mathbf{q}}$ and $\theta_{\mathbf{q}}$ the polar angle of the wave vector \mathbf{q}

Berry phase

$$\gamma_{\xi} = i \oint_{C_{mn}^{\xi}} d\mathbf{q} \cdot \langle \Psi_{\pm}(\mathbf{K}_{mn}^{\xi} + \mathbf{q}) | \nabla_{\mathbf{q}} | \Psi_{\pm}(\mathbf{K}_{mn}^{\xi} + \mathbf{q}) \rangle = \xi \pi$$

Opposite signs for different valleys!

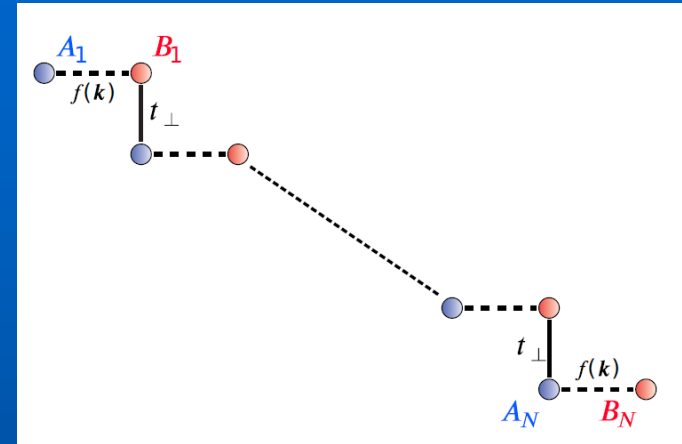
Berry phase in STM II

Rhombohedral N-layer graphene

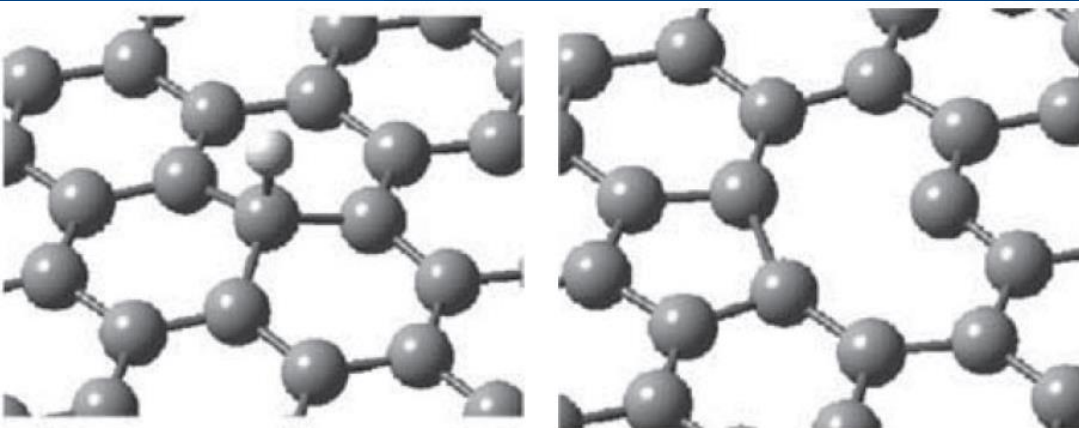
$$E_{\pm}(\mathbf{K}_{mn}^{\xi} + \mathbf{q}) \simeq \pm t_{\perp} \left(\frac{v_F}{t_{\perp}} q \right)^N$$

$$\Psi_{\pm}(\mathbf{K}_{mn}^{\xi} + \mathbf{q}) \simeq \frac{1}{\sqrt{2}} \begin{pmatrix} 1 \\ \mp \xi^N e^{-iN\mathbf{K}_{mn}^{\xi} \cdot \mathbf{d}_3} e^{-iN\theta^{\xi}(\mathbf{q})} \end{pmatrix}$$

Berry phases $\xi N \pi$



To induce intervalley transitions one need atomically sharp defects (vacancy, H adatom...)



Optimized atomic structure
Yazyev & Helm, Phys. Rev.
B 2007

Berry phase in STM III

Friedel oscillations (local perturbation, onsite only)

$$\delta\rho(\mathbf{r},\omega) = -\frac{1}{\pi} \text{Im}[\text{Tr} \delta\mathcal{G}(\mathbf{r},\mathbf{r},\omega)]$$

$$\delta\mathcal{G}(\mathbf{r}_1,\mathbf{r}_2,\omega) = G^{(0)}(\mathbf{r}_1,\omega)T(\omega)G^{(0)}(-\mathbf{r}_2,\omega)$$

$$G^{(0)}(\mathbf{k},\omega) = [\omega I - H(\mathbf{k})]^{-1}$$

$$T(\omega) = \left(1 - V \int_{BZ} G^{(0)}(\mathbf{k},\omega)\right)^{-1} V$$

Parameters for H adatoms
(or CH_3 , C_2H_5 etc. group)

PRL 105, 056802 (2010)

PHYSICAL REVIEW LETTERS

week ending
30 JULY 2010

Resonant Scattering by Realistic Impurities in Graphene

T. O. Wehling,^{1,*} S. Yuan,² A. I. Lichtenstein,¹ A. K. Geim,³ and M. I. Katsnelson²

$$\hat{H} = \sum_{ij} t_{ij} \hat{c}_i^+ \hat{c}_j + \sum_{ij} \gamma_{ij} (\hat{c}_i^+ \hat{d}_j + \hat{d}_j^+ \hat{c}_i) + E_d \sum_i \hat{d}_i^+ \hat{d}_i$$

Ab initio parameters

$$\gamma \approx 2|t|, \quad E_d \approx -\frac{|t|}{16}$$

$$V(E) = \frac{\gamma^2}{E - E_d}$$

$$\gamma^2 \gg |E_d||t|$$

infinite local repulsion

$$V = \infty \text{ and}$$

$$T_{00}(E) = -\frac{1}{G_{00}^{(0)}(E)}$$

Berry phase in STM IV

Analytic expressions

$$\delta\rho_{A_1}(\mathbf{r}, \omega) \simeq -\frac{1}{\pi} \text{Im} \left\{ i \frac{t(\omega)}{4^2 N^2 \omega^{2-3/N}} \frac{e^{i2\omega^{1/N} r}}{r} \cos(\Delta\mathbf{K} \cdot \mathbf{r}) \left[1 - \frac{i}{4} \frac{1}{\omega^{1/N} r} + \dots \right] \right\}$$

$$\delta\rho_{B_N}(\mathbf{r}, \omega) \simeq -\frac{1}{\pi} \text{Im} \left\{ i \frac{t(\omega)}{4^2 N^2 \omega^{2-3/N}} \frac{e^{i2\omega^{1/N} r}}{r} \cos[\Delta\mathbf{K} \cdot \mathbf{r} - N\Delta\theta(\mathbf{r})] (\xi\xi')^N \left[1 + i \left(N^2 - \frac{1}{4} \right) \frac{1}{\omega^{1/N} r} + \dots \right] \right\}$$

$$N\Delta\theta(\mathbf{r}) = N\Delta\mathbf{K} \cdot \mathbf{d}_3 + N(\xi - \xi')\theta_{\mathbf{r}} - N\xi'\pi$$

Numerical results

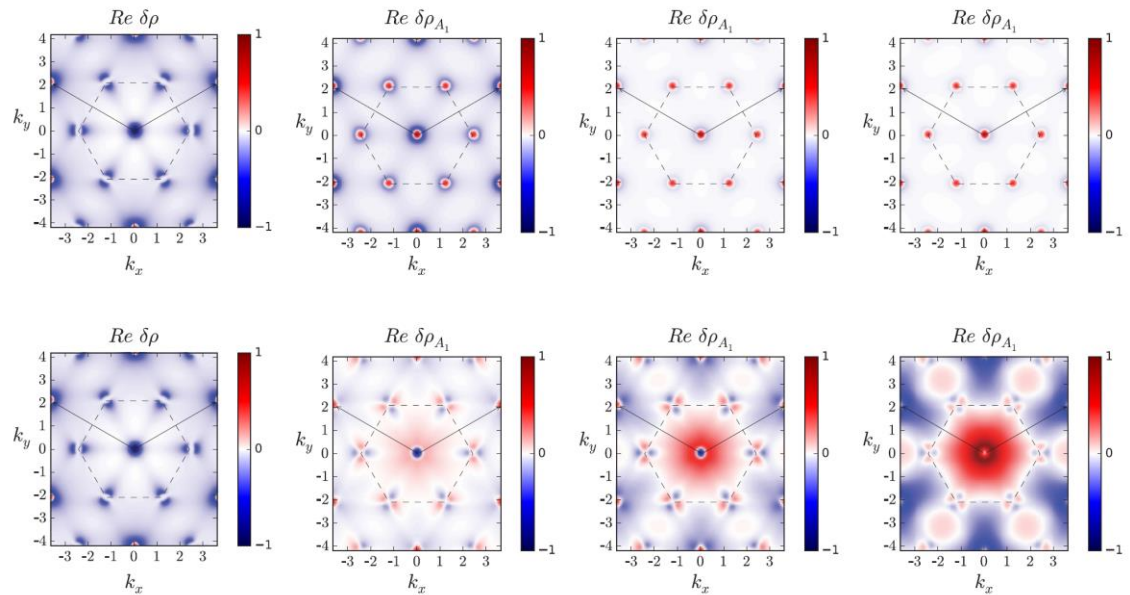


FIG. 8. Momentum space pattern of the LDOS on the impurity surface for $N = 1, 2, 3$, and 4 (from left to right). Only the real part of the LDOS Fourier transform is depicted when the impurity is located on sublattice A_1 (first row) and B_1 (second row). The potential magnitude is $V_0 = t$. Note that $\delta\rho = \delta\rho_{A_1} + \delta\rho_{B_1}$ in the case of monolayer graphene, whereas the LDOS modulations on the impurity surface are given by $\delta\rho_{A_1}$ otherwise. The dashed-line-made hexagons outline the Brillouin zone and can be used as guides for the eyes. The two vectors that span the reciprocal space are depicted by black arrows. The scattering which occurs between equivalent valleys yields the spots that can be connected to the origin by a linear combination of these basis vectors. They mainly have a circular symmetry. The spots at the hexagon corners are induced by scattering between nonequivalent valleys ($\xi = -\xi'$). They have a twofold rotational symmetry when the impurity is localized on sublattice B_1 (second row).

Berry phase in STM V

Analysis in k -space (Fourier transform of total density)

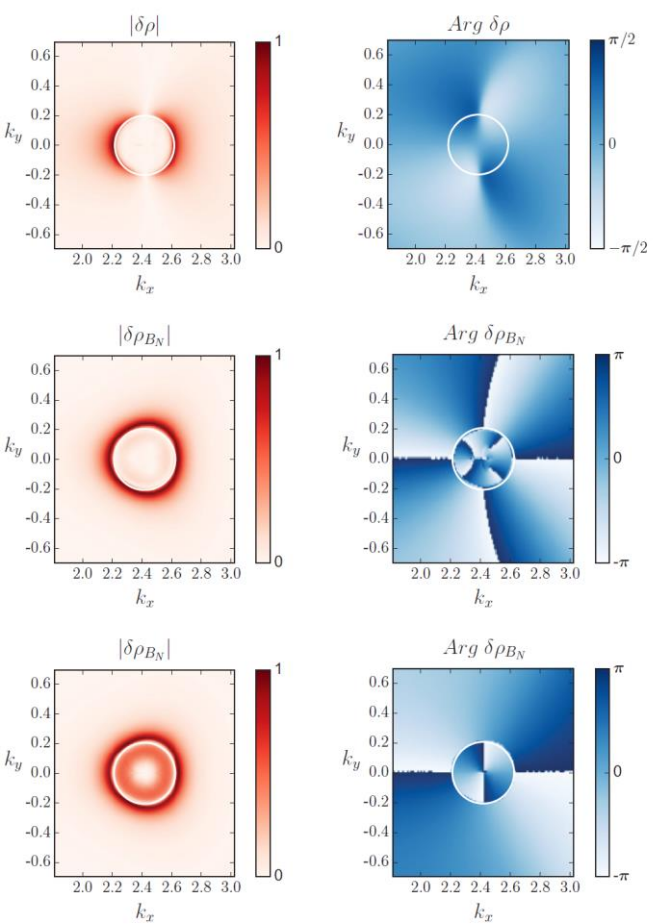


FIG. 11. Polar representation of the LDOS Fourier transform induced by the scattering between nonequivalent valleys on the pristine surface. It is illustrated for the valleys that are related to one another by $\delta m = 1$, $\delta n = -1$, and $\xi = -\xi' = -1$. The $2q_F$ -radius circle is mentioned in white as a guide for the eyes. The first row refers to the impurity surface of monolayer graphene ($N = 1$) and thus $\delta\rho = \delta\rho_{A_1} + \delta\rho_{B_1}$. The second and third rows are both obtained for bilayer graphene when the impurity lies on sublattice A_1 and B_1 , respectively. In both cases the LDOS modulations on the pristine surface mainly involve sublattice B_N at low energy, so that only $\delta\rho_{B_N}$ is mentioned.

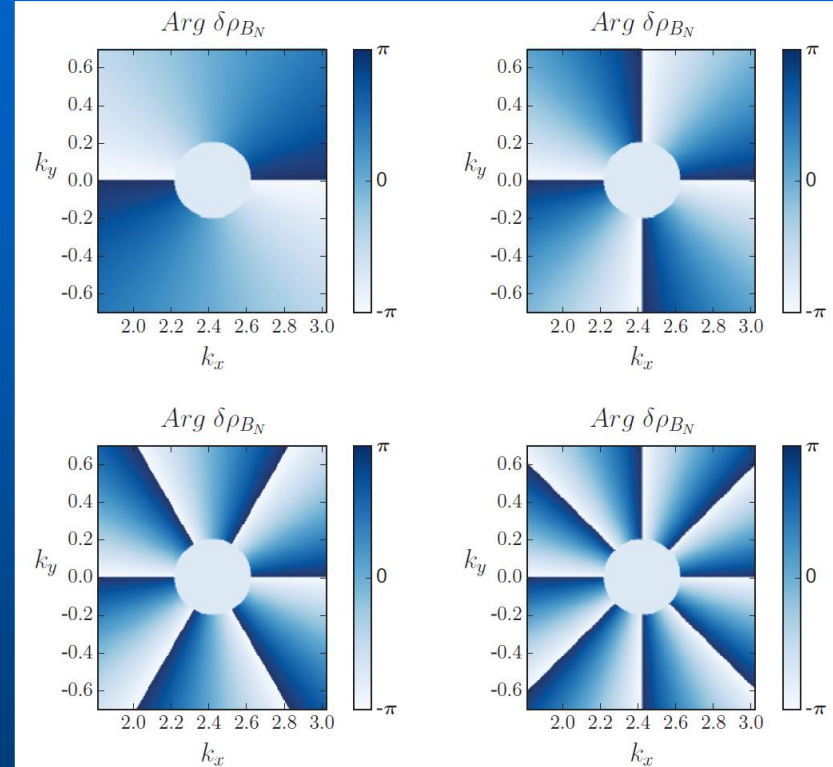


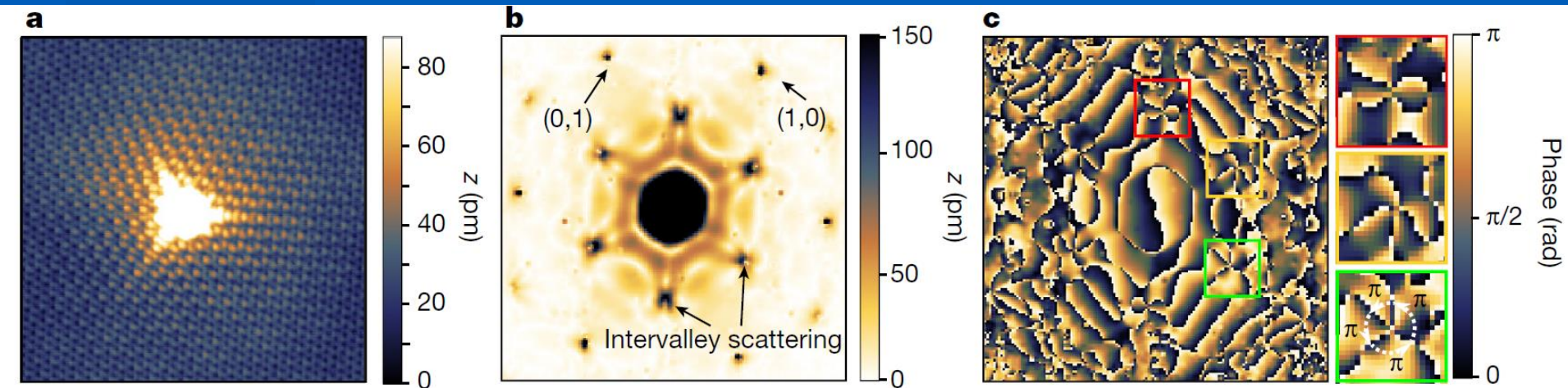
FIG. 12. Argument of the LDOS Fourier transform due to scattering between nonequivalent valleys for $N = 1$ (top left-hand corner), $N = 2$ (top right-hand corner), $N = 3$ (bottom left-hand corner), and $N = 4$ (bottom right-hand corner). This multivalued function, obtained from the analytic expression (68), winds $2N$ times when the wave vector describes a closed path that encloses once the $2q_F$ -radius ring. This winding number leads to the Berry phase difference between the two nonequivalent valleys involved in the scattering.

Berry phase in STM: Experiment

Measuring the Berry phase of graphene from wavefront dislocations in Friedel oscillations

C. Dutreix^{1*}, H. González-Herrero^{2,3}, I. Brihuega^{2,3,4}, M. I. Katsnelson⁵, C. Chapelier⁶ & V. T. Renard^{6*}

10 OCTOBER 2019 | VOL 574 | NATURE | 219



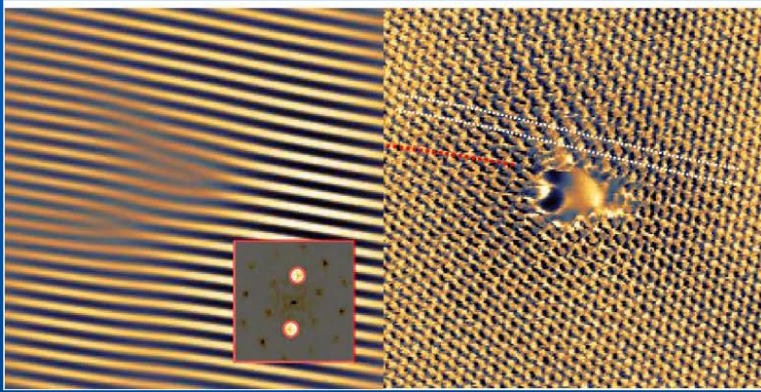
Friedel oscillations near a H atom

a, Topography STM image of a H adatom at the surface of graphene. The image is $10 \text{ nm} \times 10 \text{ nm}$ in size. The tunnelling bias is $V_b = 0.4 \text{ V}$ and the tunnelling current is $i_t = 45.5 \text{ pA}$. **b**, Modulus of the fast Fourier transform (FFT) of the image in **a**. The points labelled (1, 0) and (0, 1) correspond to the atomic signal. **c**, Phase of the FFT of the image in **a**. Magnifications of the inter-valley backscattering signal are presented on the right, with corresponding border colours red, yellow and green.

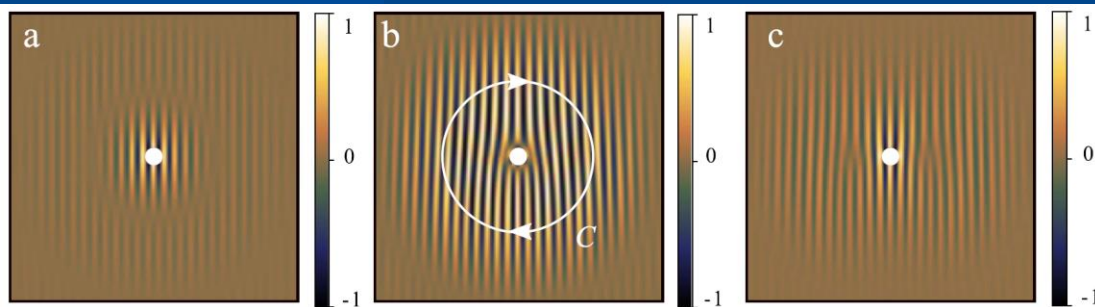
Wavetrain dislocations

Nye, J. F. & Berry, M. V. Dislocations in wave trains. *Proc. R. Soc. Lond. A* **336**, 165–190 (1974).

Suggested for sound waves; claimed to be non-observable for quantum waves – interference between two valleys make them observable



Raw image (right) Fourier filtered to separate intervalley contribution only; wave train dislocations are clearly visible



Two dislocations are visible on the panel b

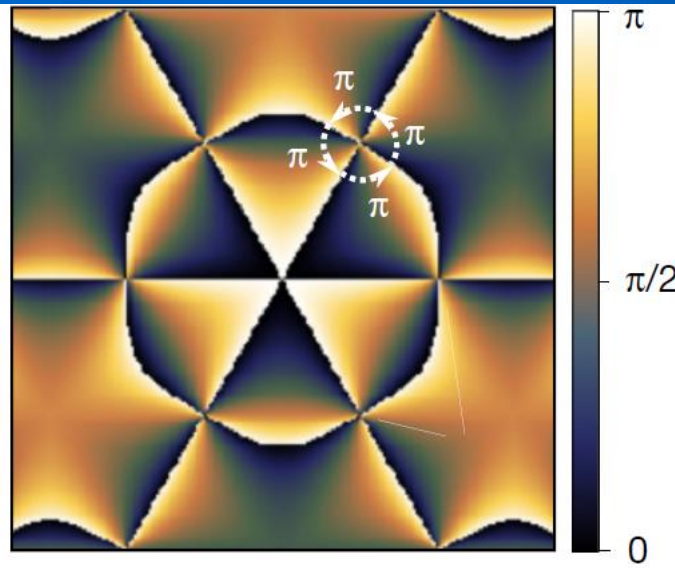
Dutreix *et al.*

*Comptes Rendus
Physique*

<https://doi.org/10.5802/crphys.79>

Figure 5. (a) Charge density modulation induced by intervalley scattering on sublattice A. (b) Charge density modulation induced by intervalley scattering on sublattice B. (c) Total charge density modulation induced by intervalley scattering and resulting from the two sublattice contributions. The modulations have been normalized to 1. The images are 10 nm × 10 nm and the signal is integrated from 0 eV to $V_b = 0.4$ eV. The white disk depicts the H adatom. The figure is adapted from Ref. [31].

Wavetrain dislocations II



Hydrogen atom in sublattice A

$$\delta\rho(\Delta\mathbf{K}, \mathbf{r}, V_b) = \delta\rho_A(r, V_b) \cos(\Delta\mathbf{K} \cdot \mathbf{r}) + \xi\xi' \delta\rho_B(r, V_b) \cos(\Delta\mathbf{K} \cdot \mathbf{r} - (\xi - \xi')\theta_{\mathbf{r}})$$

on sublattice B has an additional phase shift $-2\theta_{\mathbf{r}}$ which is nothing but the pseudospin rotation

Theoretical density modulation: Fourier transform of $\Delta\rho(\mathbf{r})$

The strength N of the dislocation is then given by the vortex charge, that is, the circulation of the gradient phase of the $\Delta\mathbf{K}$ -wavevector oscillations around the adatom:

$$2\pi N = \oint_C \mathbf{dr} \cdot \nabla_{\mathbf{r}}(\Delta\mathbf{K} \cdot \mathbf{r} - 2\xi\theta_{\mathbf{r}}) = -2 \oint_C \mathbf{dr} \cdot \nabla_{\mathbf{r}}(\xi\theta_{\mathbf{r}}) = 4\pi. \quad (5)$$

This explains the $N = 2$ wavefronts emerging from the H adatom in Figure 5b and shows explicitly that they reveal the pseudospin winding and so the Berry phase. This double dislocation splits into two single dislocations in the experiments (Figure 3d). This particular feature is recovered when taking into account the contributions of the two sublattices in the STM signal, as shown in Figure 5c.

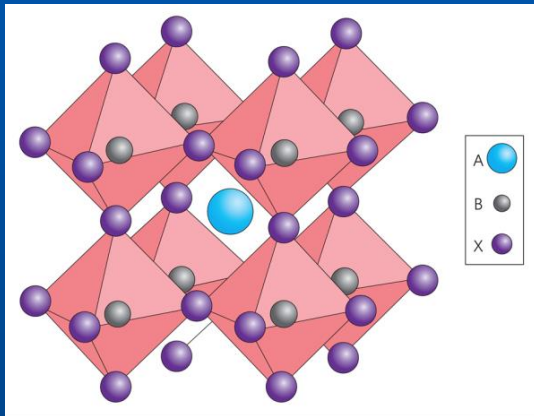
Observation of dislocations visualize winding number

III. Self-induced spin glass state

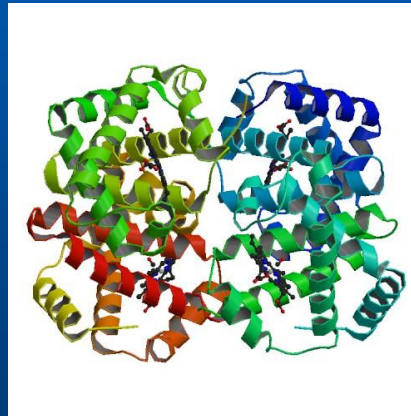
The problem: Origin of complexity

Schrödinger: life substance is “aperiodic crystal”

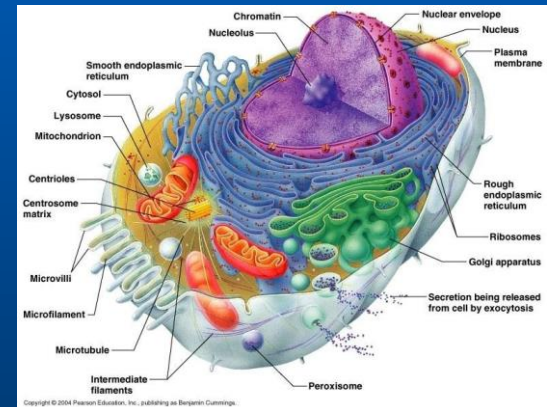
Intuitive feeling: crystals are simple, biological structures are complex



Crystals

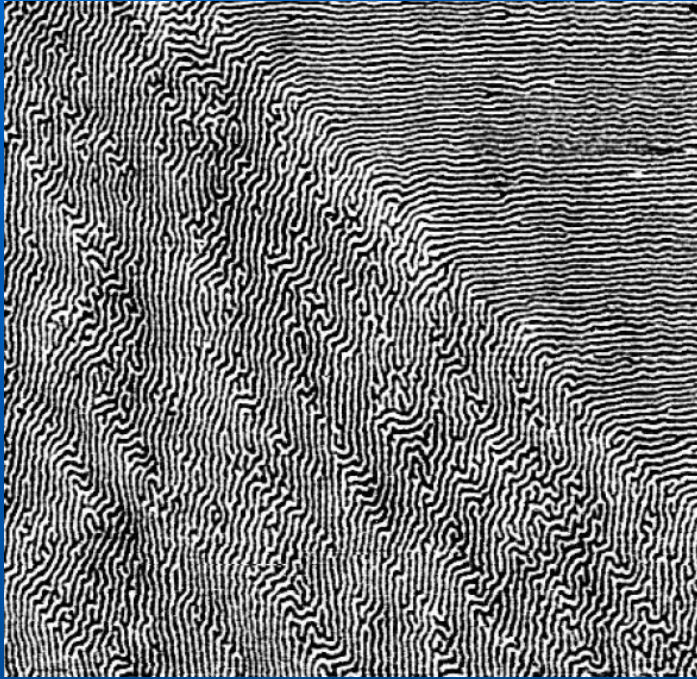


Biomolecules



Organelles

Complexity (“patterns”) in inorganic world

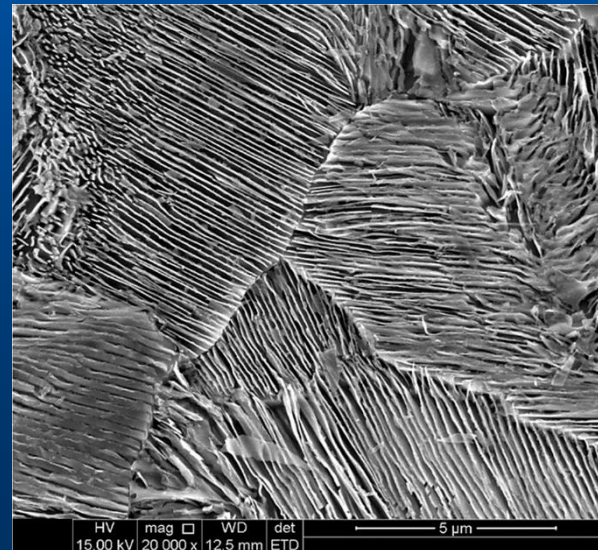


Stripe domains in ferromagnetic thin films

Microstructures in metals and alloys



Stripes on a beach in tide zone



Pearlitic structure in rail steel (Sci Rep 9, 7454 (2019))

Do we understand this? No, or, at least, not completely

Magnetic patterns

Example: strip domains in thin ferromagnetic films

PHYSICAL REVIEW B 69, 064411 (2004)

Magnetization and domain structure of bcc $\text{Fe}_{81}\text{Ni}_{19}/\text{Co}$ (001) superlattices

R. Bručas, H. Hafermann, M. I. Katsnelson, I. L. Soroka, O. Eriksson, and B. Hjörvarsson

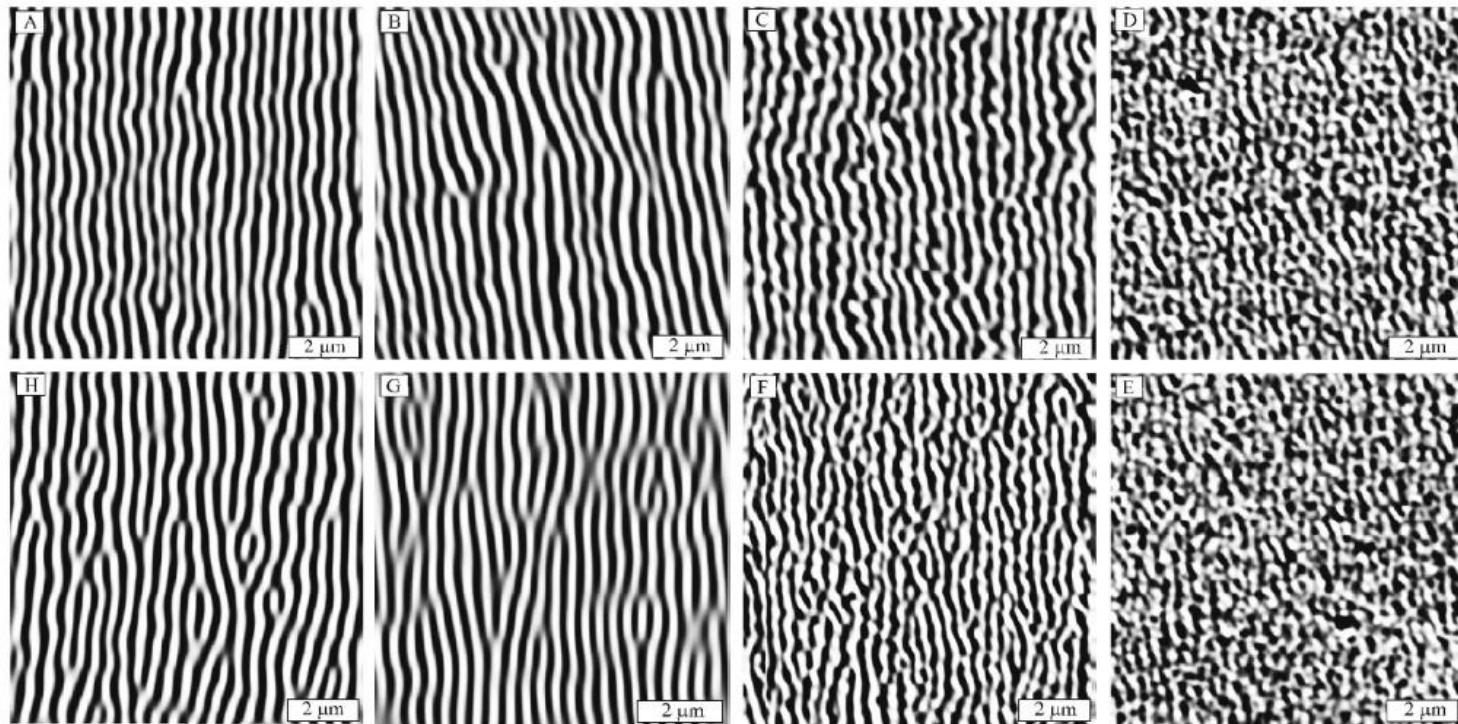
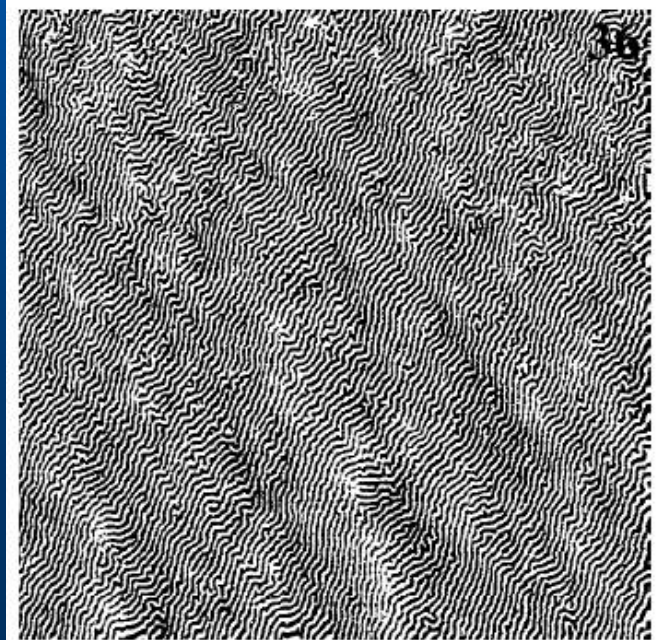
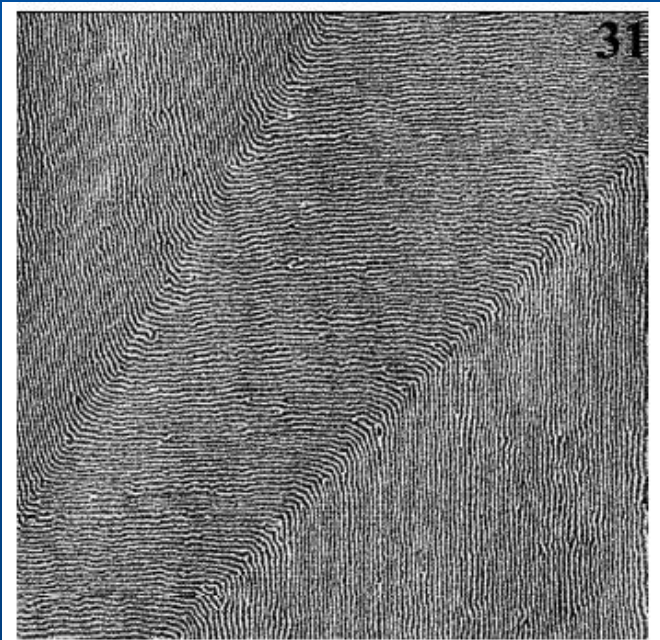
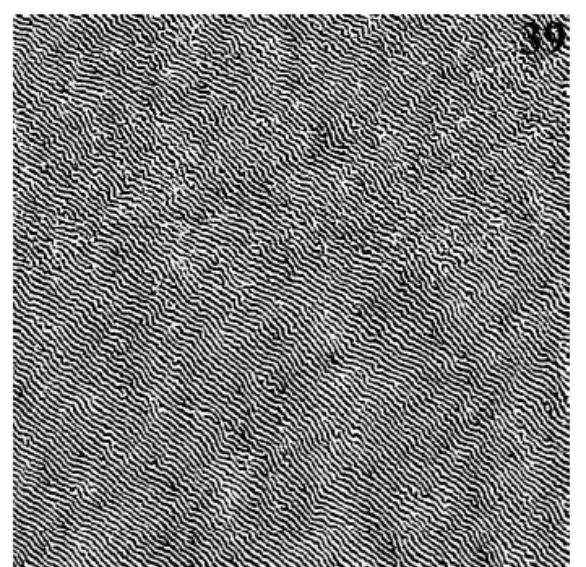
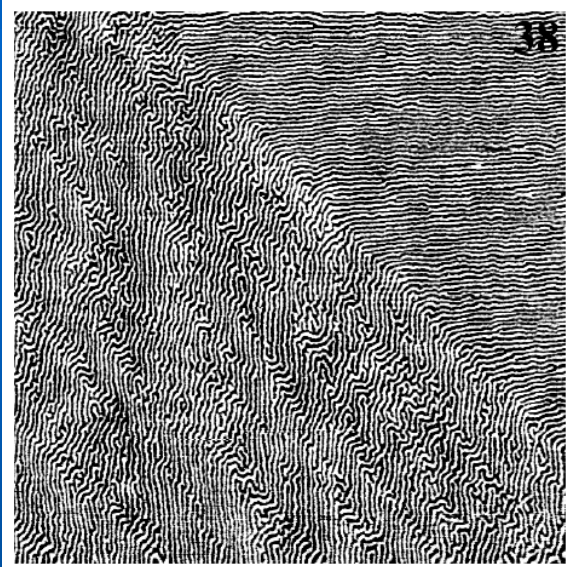
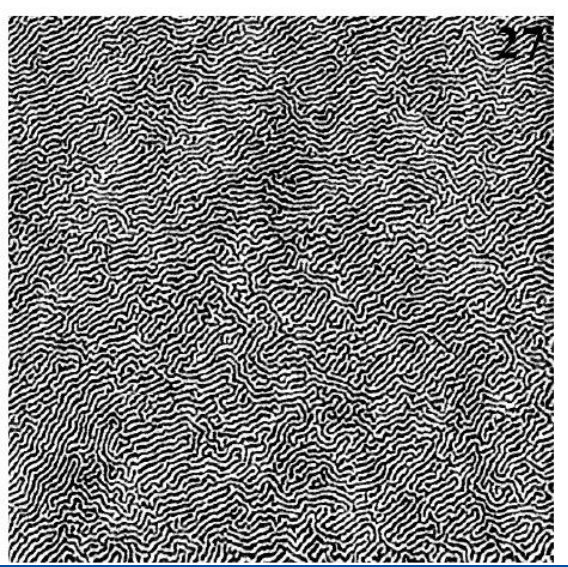


FIG. 2. The MFM images of the 420 nm thick $\text{Fe}_{81}\text{Ni}_{19}/\text{Co}$ superlattice at different externally applied in-plane magnetic fields: (a)—virgin (nonmagnetized) state; (b), (c), (d)—increasing field 8.3, 30, and 50 mT; (e), (f), (g)—decreasing field 50, 30, 8.3 mT; (h)—in remanent state.

Magnetic patterns II



Magnetic patterns III

Europhys. Lett., **73** (1), pp. 104–109 (2006)

DOI: 10.1209/epl/i2005-10367-8

Topological defects, pattern evolution, and hysteresis
in thin magnetic films

P. A. PRUDKOVSKII¹, A. N. RUBTSOV¹ and M. I. KATSNELSON²

$$H = \int \left(\frac{J_x}{2} \left(\frac{\partial \mathbf{m}}{\partial x} \right)^2 + \frac{J_y}{2} \left(\frac{\partial \mathbf{m}}{\partial y} \right)^2 - \frac{K}{2} m_z^2 - h m_y \right) d^2 r + \\ + \frac{Q^2}{2} \int \int m_z(\mathbf{r}) \left(\frac{1}{|\mathbf{r} - \mathbf{r}'|} - \frac{1}{\sqrt{d^2 + (\mathbf{r} - \mathbf{r}')^2}} \right) m_z(\mathbf{r}') d^2 r d^2 r'.$$

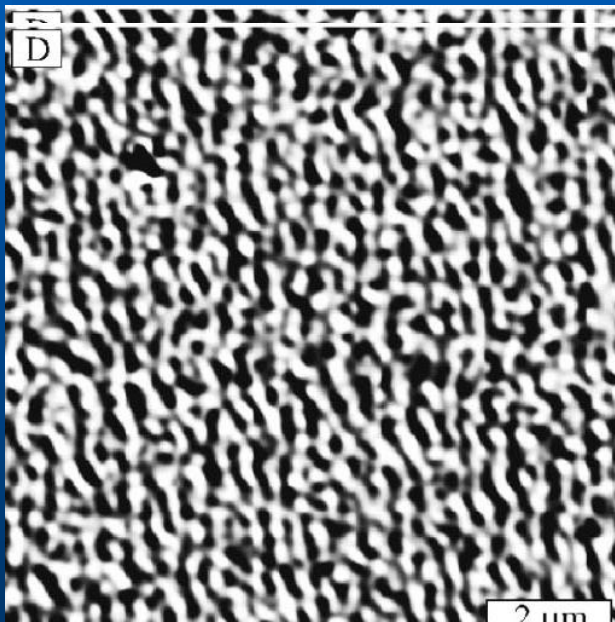
Competition of exchange interactions (want homogeneous ferromagnetic state) and magnetic dipole-dipole interactions (want total magnetization equal to zero)

Competing interactions and self-induced spin glasses

Special class of patterns: “chaotic” patterns

Hypothesis: a system wants to be modulated but cannot decide in which direction

PHYSICAL REVIEW B 69, 064411 (2004)



$$E_m = \int \int d\mathbf{r} d\mathbf{r}' m(\mathbf{r}) m(\mathbf{r}') \left[\frac{1}{|\mathbf{r} - \mathbf{r}'|} - \frac{1}{\sqrt{(\mathbf{r} - \mathbf{r}')^2 + D^2}} \right]$$
$$= 2\pi \sum_{\mathbf{q}} m_{\mathbf{q}} m_{-\mathbf{q}} \frac{1 - e^{-qD}}{q}, \quad (13)$$

where $m_{\mathbf{q}}$ is a two-dimensional Fourier component of the magnetization density. At the same time, the exchange energy can be written as

$$E_{exch} = \frac{1}{2} \alpha \sum_{\mathbf{q}} q^2 m_{\mathbf{q}} m_{-\mathbf{q}}, \quad (14)$$

so there is a finite value of the wave vector $q = q^*$ found from the condition

$$\frac{d}{dq} \left(2\pi \frac{1 - e^{-qD}}{q} + \frac{1}{2} \alpha q^2 \right) = 0 \quad (15)$$

Self-induced spin glasses II

PHYSICAL REVIEW B 93, 054410 (2016)

Stripe glasses in ferromagnetic thin films

Alessandro Principi* and Mikhail I. Katsnelson

PRL 117, 137201 (2016)

PHYSICAL REVIEW LETTERS

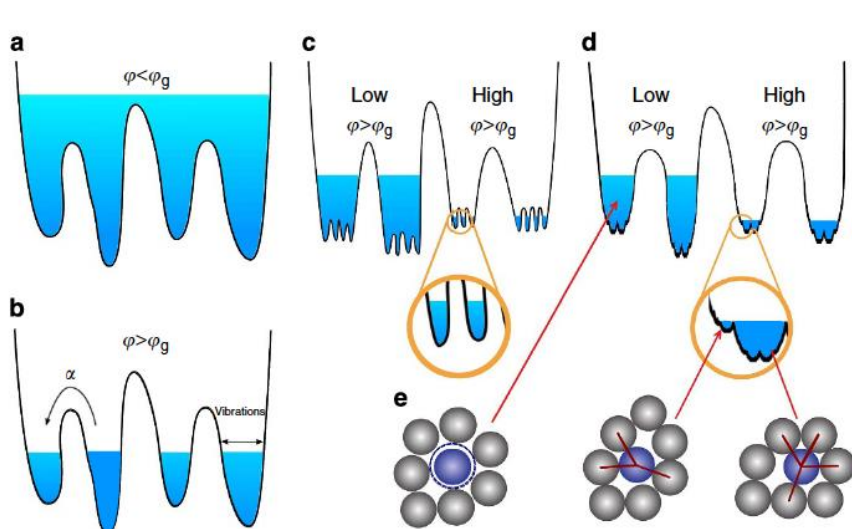
week ending
23 SEPTEMBER 2016

Self-Induced Glassiness and Pattern Formation in Spin Systems Subject to Long-Range Interactions

Alessandro Principi* and Mikhail I. Katsnelson

Development of idea of stripe glass, J. Schmalian and P. G. Wolynes, PRL 2000

Glass: a system with an energy landscape characterizing by infinitely many local minima, with a broad distribution of barriers, relaxation at “any” time scale and aging (at thermal cycling you never go back to exactly the same state)



Picture from P. Charbonneau et al,

DOI: 10.1038/ncomms4725

Intermediate state between equilibrium and non-equilibrium, opportunity for history and memory

Self-induced spin glasses III

One of the ways to describe: R. Monasson, PRL 75, 2847 (1995)

$$\mathcal{H}_\psi[m, \lambda] = \mathcal{H}[m, \lambda] + g \int dr [m(r) - \psi(r)]^2$$

The second term describes attraction of our physical field $m(r)$ to some external field $\psi(r)$

If the system can be glued, with infinitely small interaction g , to macroscopically large number of configurations it should be considered as a glass

Then we calculate

$$F_g = \frac{\int \mathcal{D}\psi Z[\psi] F[\psi]}{\int \mathcal{D}\psi Z[\psi]} \text{ and see whether the limits}$$

$$F_{\text{eq}} = \lim_{N \rightarrow \infty} \lim_{g \rightarrow 0} F_g$$

and

$$F = \lim_{g \rightarrow 0} \lim_{N \rightarrow \infty} F_g$$

are different

If yes, this is self-induced glass

No disorder is needed (contrary to traditional view on spin glasses)

Self-induced spin glasses IV

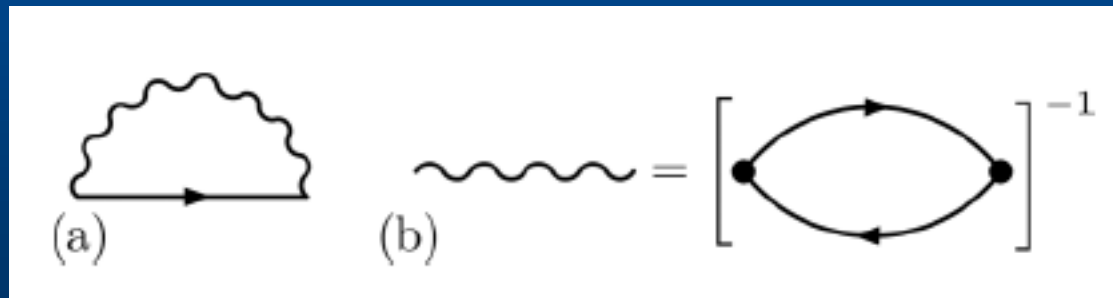
PHYSICAL REVIEW B 93, 054410 (2016)

Stripe glasses in ferromagnetic thin films

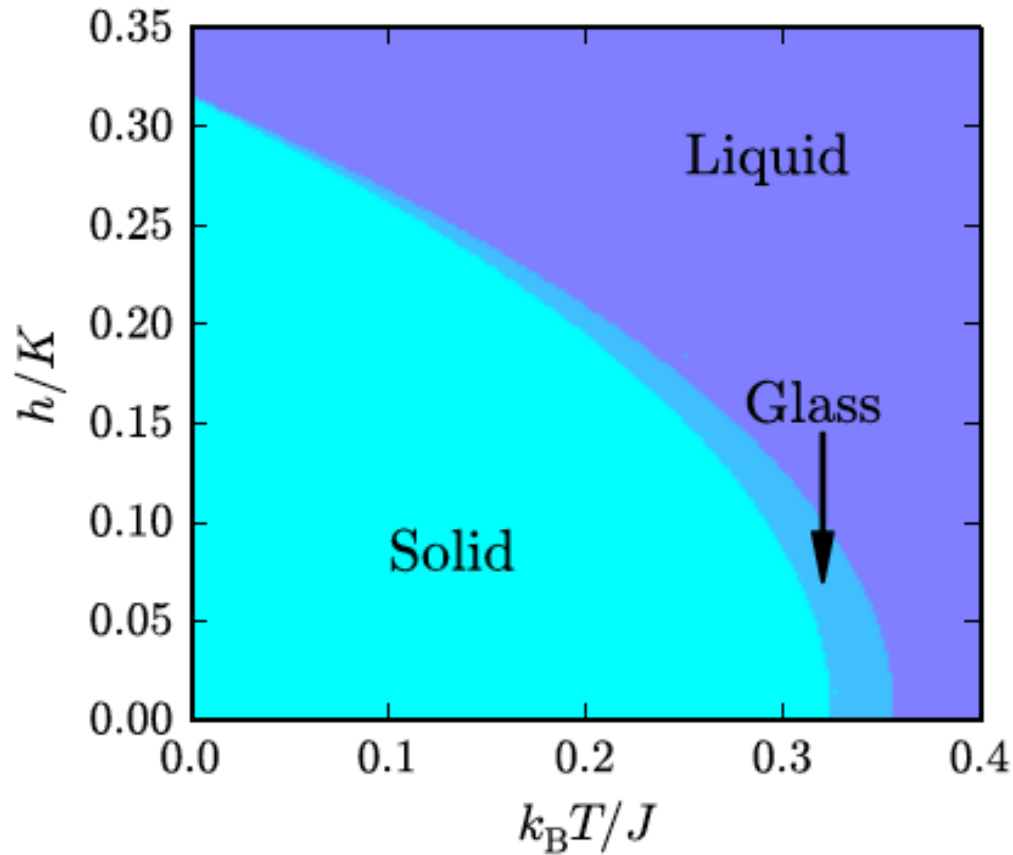
Alessandro Principi* and Mikhail I. Katsnelson

$$\begin{aligned}\mathcal{H}[m, \lambda] = & \int dr \{ J [\partial_i m_j(r)]^2 - K m_z^2(r) - 2h(r) \cdot m(r) \} \\ & + \frac{Q}{2\pi} \int dr dr' m_z(r) \\ & \times \left[\frac{1}{|r - r'|} - \frac{1}{\sqrt{d^2 + |r - r'|^2}} \right] m_z(r') \\ & + \int dr \{ \lambda(r) [m^2(r) - 1] \}.\end{aligned}\quad (1)$$

Self-consistent screening approximation for spin propagators



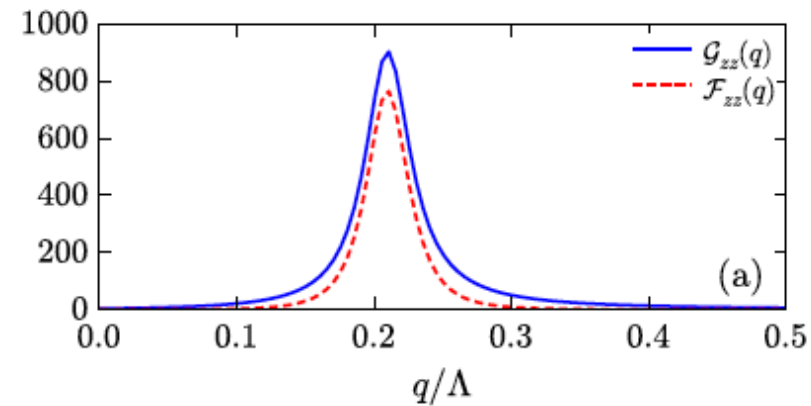
Self-induced spin glasses V



Phase diagram

Maximum at

$$q_0 \simeq [Q/(2J)]^{1/3} \neq 0$$



q-dependence of normal and anomalous ("glassy", non-ergodic) spin-spin correlators

Self-induced spin glasses VI

PRL 117, 137201 (2016)

PHYSICAL REVIEW LETTERS

week ending
23 SEPTEMBER 2016

Self-Induced Glassiness and Pattern Formation in Spin Systems Subject to Long-Range Interactions

Alessandro Principi* and Mikhail I. Katsnelson

Maximal simplification
(Brazovskii model)

$$\mathcal{F} = \frac{1}{2} \sum_{\mathbf{q}} G_0^{-1}(\mathbf{q}) s_{\mathbf{q}} \cdot s_{-\mathbf{q}} + i \sum_i \sigma_i (s_i^2 - 1)$$

$$G_0^{-1}(\mathbf{q}) = q_0^D (q^2 / q_0^2 - 1)^2 / 4 + q_0^D \varepsilon_0^2 \sin^2(\theta_q)$$

Spin-glass state exists!

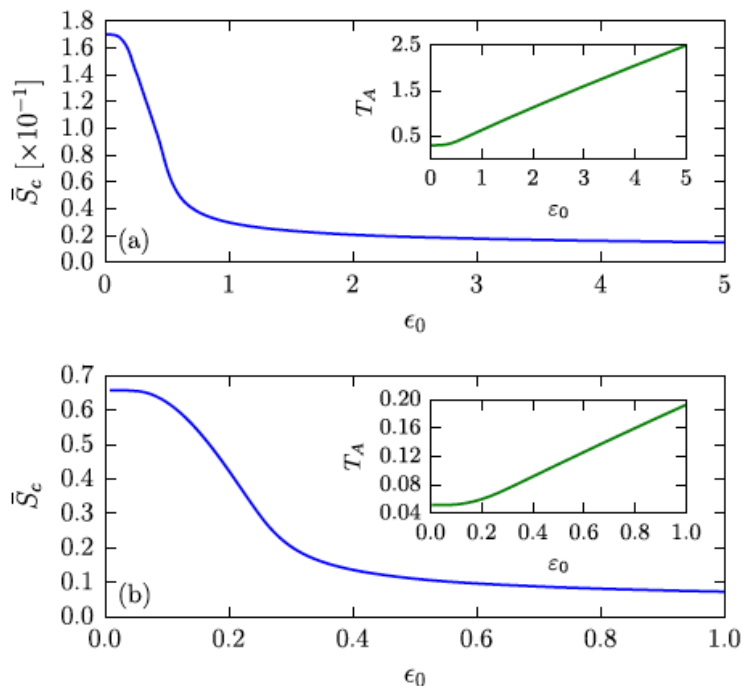


FIG. 2. Panel (a) the configurational entropy of the mean-field problem for the two-dimensional Ising model ($D = 2$ and $N_s = 1$). Note that this curve has been multiplied by a factor 0.1. Inset: the transition temperature T_A as a function of the anisotropy parameter ε_0 . Panel (b) same as panel (a) but for the two-dimensional Heisenberg model ($D = 2$, $N_s = 3$). Inset: the temperature T_A as a function of ε_0 .

Experimental observation of self-induced spin glass state: elemental Nd

Self-induced spin glass state in elemental and crystalline neodymium

Umut Kamber, Anders Bergman, Andreas Eich, Diana Iuşan, Manuel Steinbrecher, Nadine Hauptmann, Lars Nordström, Mikhail I. Katsnelson, Daniel Wegner*, Olle Eriksson, Alexander A. Khajetoorians*

Science **368**, 966 (2020)

Spin-polarized STM experiment, Radboud University



Magnetic structure: no long-range

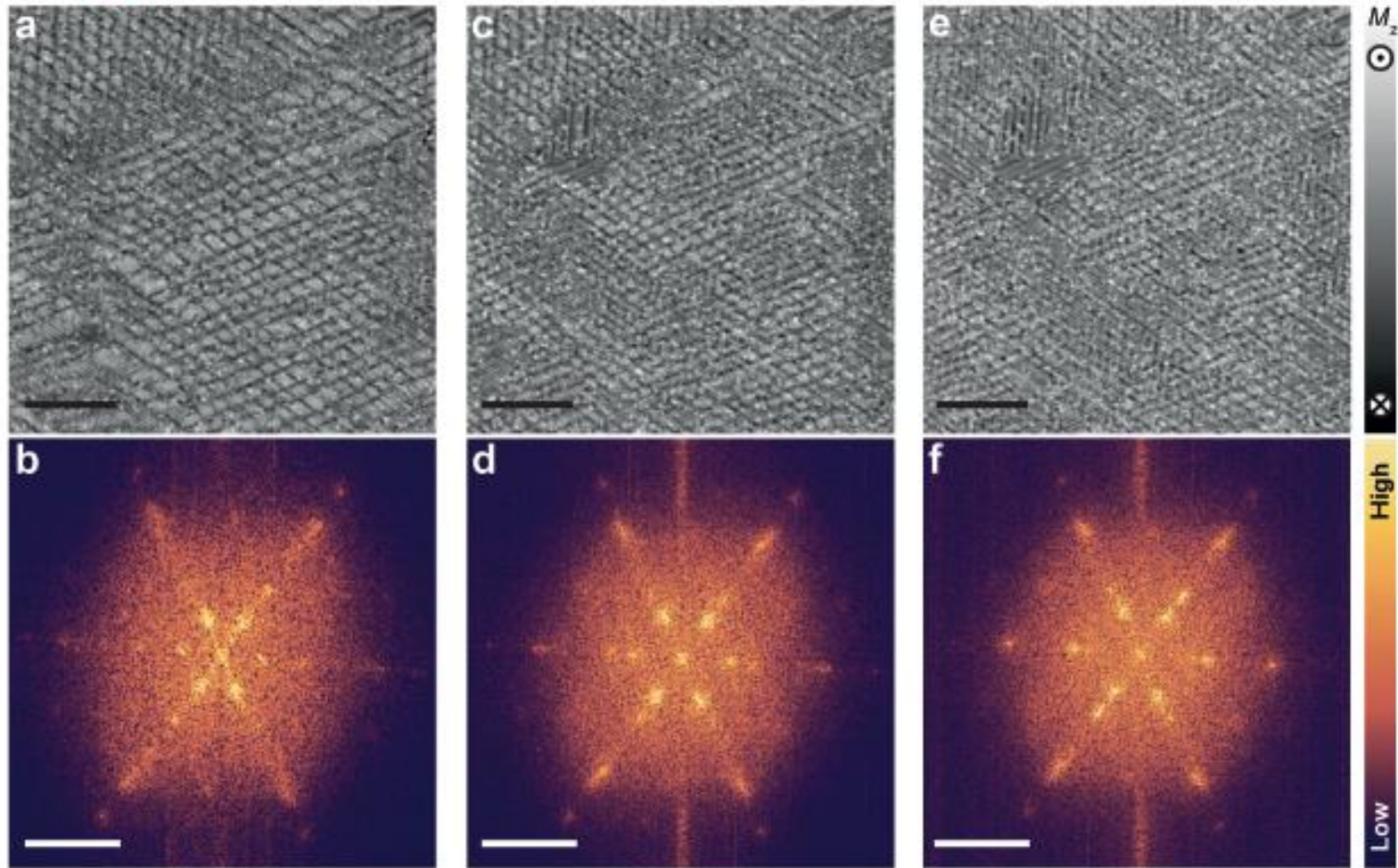


- ✓ Short-range non-collinear order
- ✗ Long-range order

Cr bulk tip

T: 1.3K
B: 0T

Magnetic structure: local correlations

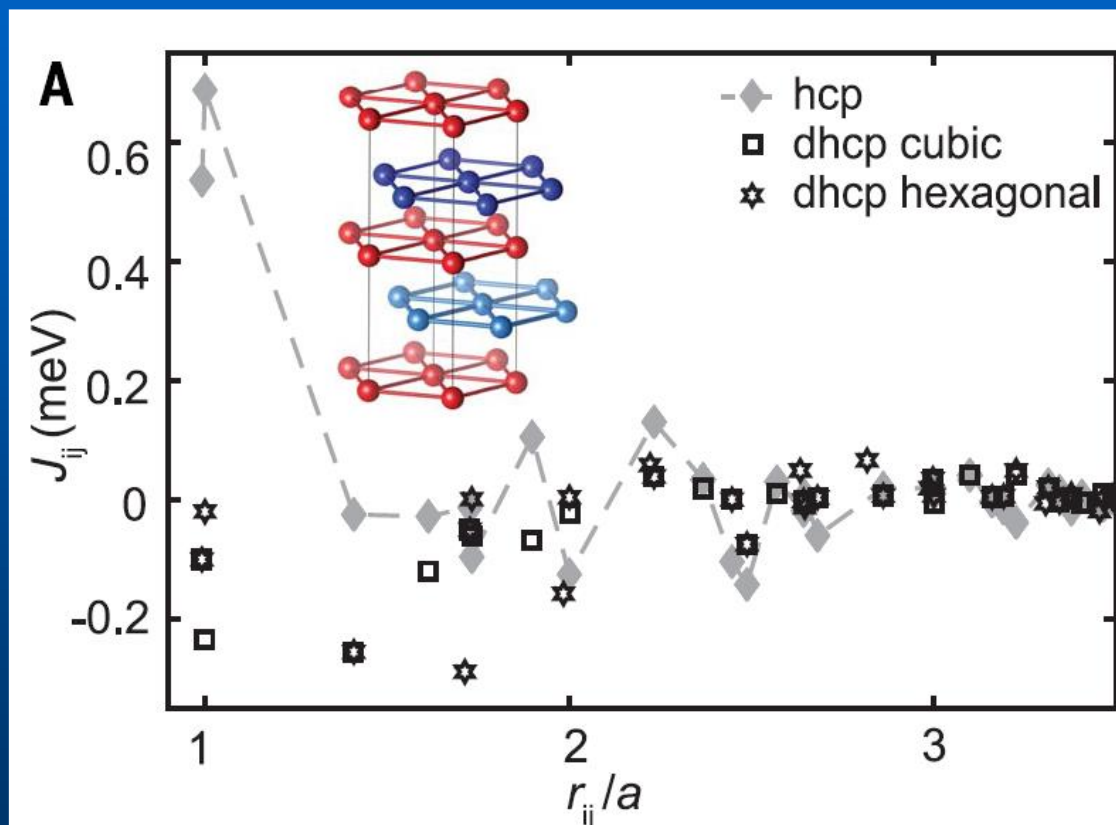


The most important observation: **aging**. At thermocycling (or cycling magnetic field) the magnetic state is not exactly reproduced

Ab initio: magnetic interactions in bulk Nd

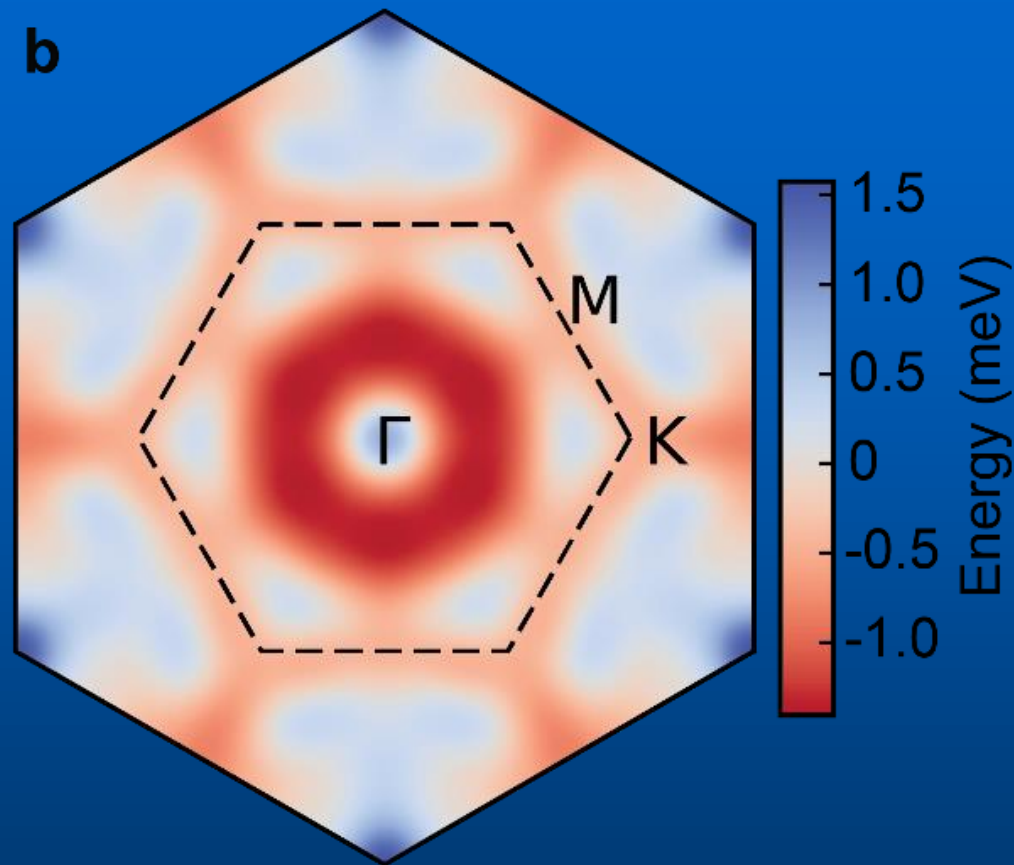
Method: magnetic force theorem (Lichtenstein, Katsnelson, Antropov, Gubanov JMMM 1987)

Calculations: Uppsala team (Olle Eriksson group)



- Dhcp structure drives competing AFM interactions
- Frustrated magnetism

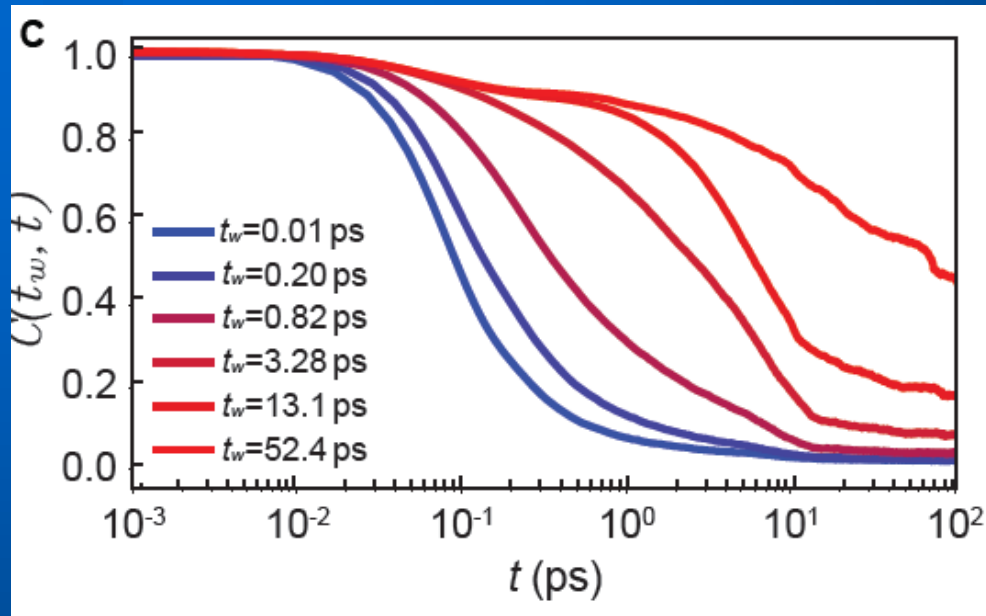
Ab initio bulk Nd: energy landscape



- $E(Q)$ landscape features flat valleys along high symmetry directions

See A. Principi, M.I. Katsnelson,
PRB/PRL (2016)/(2017)

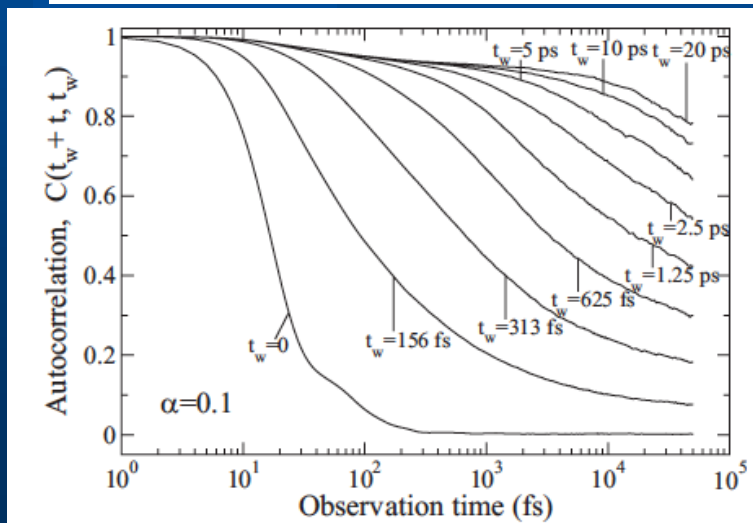
Spin-glass state in Nd: spin dynamics



Atomistic spin dynamics simulations

Typically spin-glass behavior

Autocorrelation function $C(t_w, t) = \langle \mathbf{m}_i(t + t_w) \cdot \mathbf{m}_i(t_w) \rangle$ for dhcp Nd at $T = 1$ K



To compare: the same for prototype disordered spin-glass Cu-Mn

B. Skubic et al, PRB 79, 024411 (2009)

Further development

Thermally-induced magnetic order from glassiness in elemental
neodymium

Benjamin Verihac¹, Lorena Niggli¹, Anders Bergman², Umut Kamber¹, Andrey Bagrov^{1,2}, Diana Iuşan²,
Lars Nordström², Mikhail I. Katsnelson¹, Daniel Wegner¹, Olle Eriksson^{2,3}, Alexander A.
Khajetoorians^{1*}

[arXiv:2109.04815](https://arxiv.org/abs/2109.04815)

*Glassy state at low T
and long-range order
at T increase*

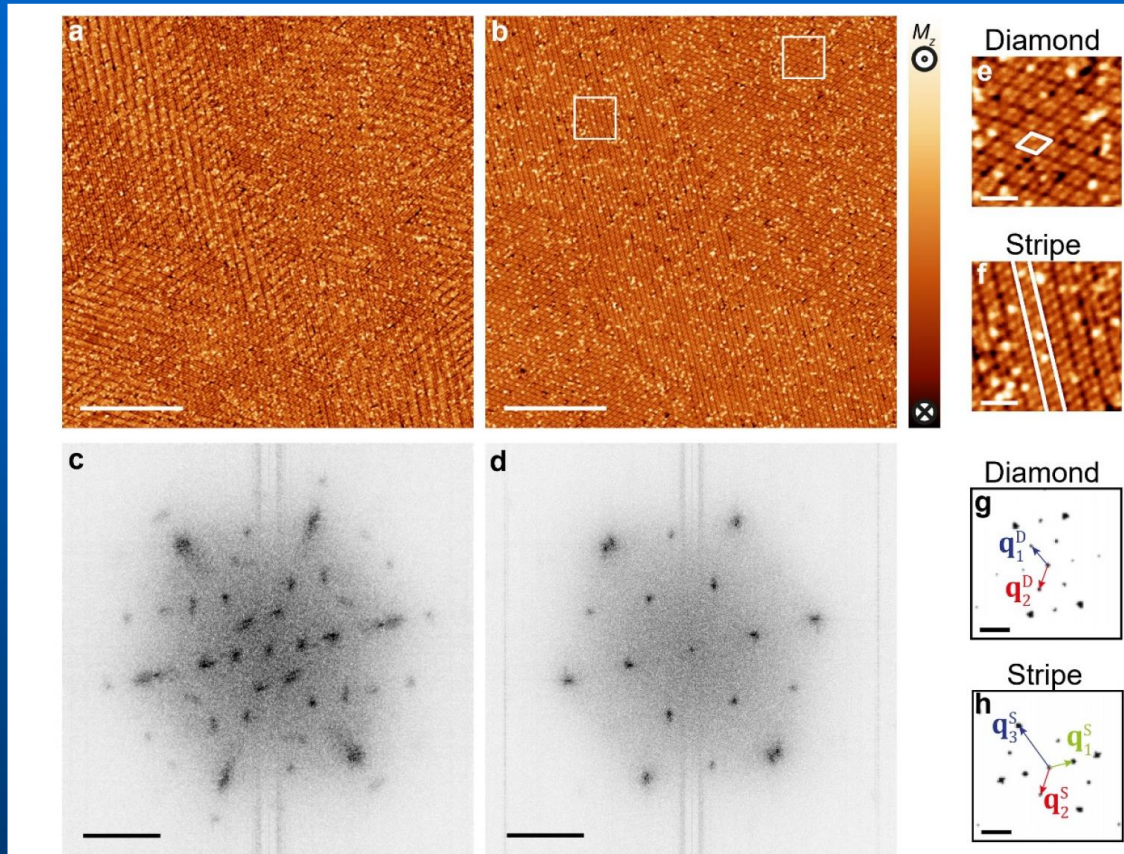
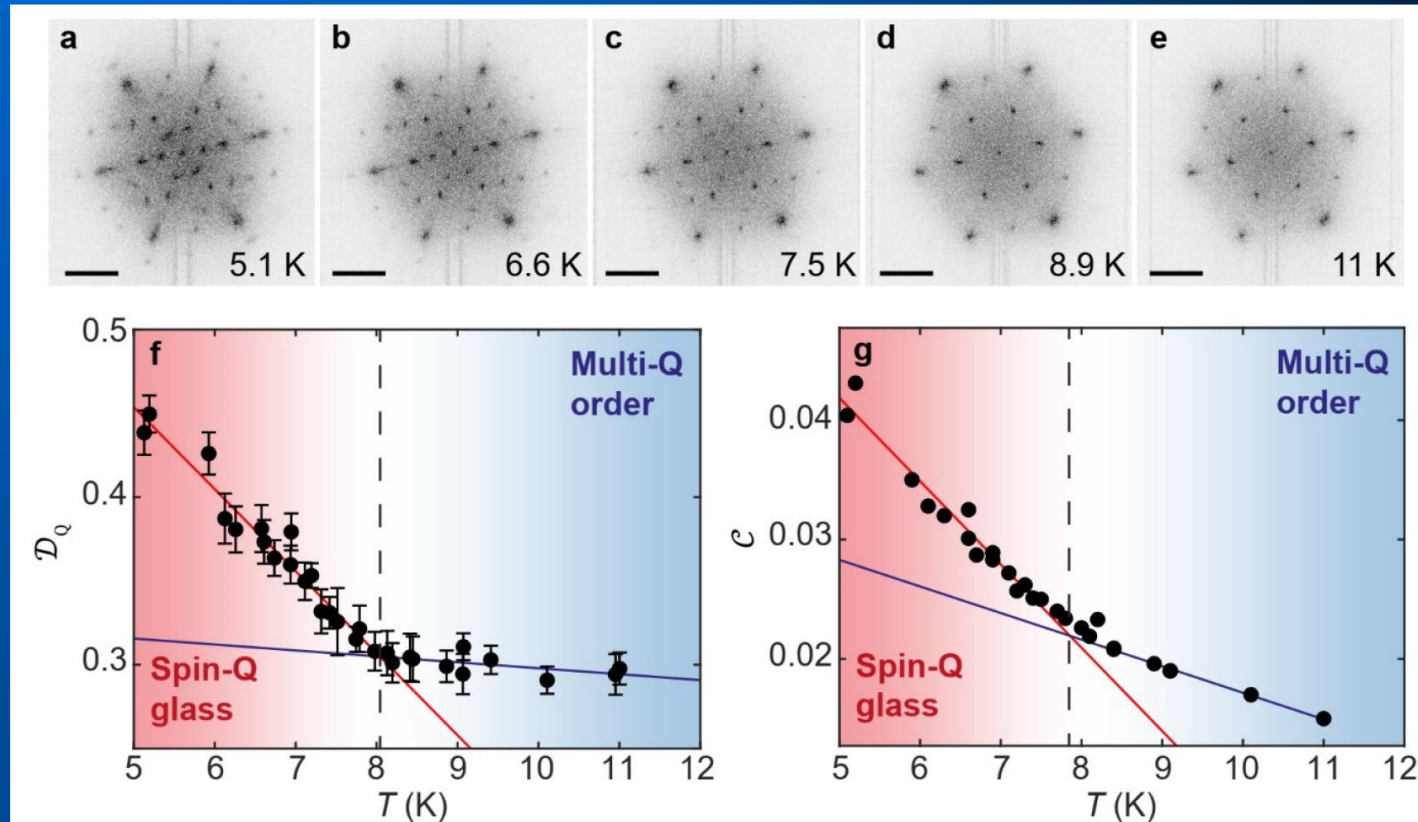


Figure 2: Emergence of long-range multi-Q order from the spin-Q glass state at elevated

temperature. a,b. Magnetization images of the same region at $T = 5.1$ K and 11 K, respectively ($I_t = 100$ pA, a-b, scale bar: 50 nm). c,d. Corresponding Q-space images (scale bars: 3 nm^{-1}), illustrating the changes from strong local (i.e. lack of long-range) Q order toward multiple large-scale domains with well-defined long-range multi-Q order. e,f. Zoom-in images of the diamond-like (e) and stripe-like (f) patterns (scale bar: 5 nm). The locations of these images is shown by the white squares in b. g,h. Display of multi-Q state maps of the two apparent domains in the multi-Q ordered phase, where (g)

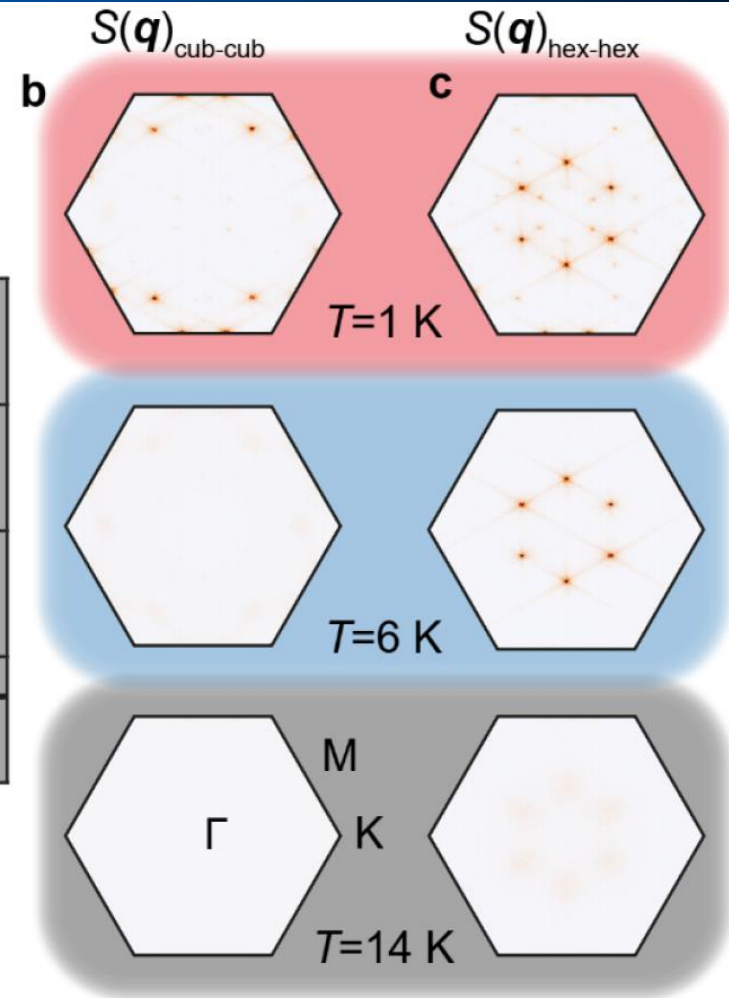
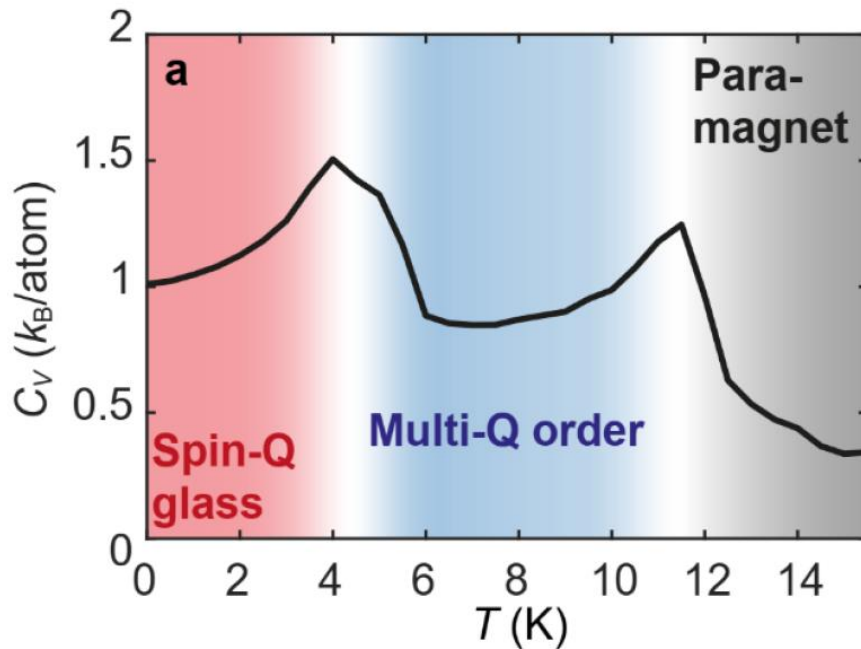
$T=5K$ (a,c): spin glass
 $T=11K$ (b,d): (noncollinear) AFM

Further development II



Phase transition at approx. 8K (seen via “complexity” measures)

Further development III



Theory: Atomistic simulations

To conclude

*STM + theory: powerful tools do study the main
Problems of contemporary physics:*

- *many-body effects*
- *topological properties*
- *pattern formation and origin for complexity*

*Many thanks to all collaborators (too many to
be all named here) and many thanks for you
attention*